

**DEVELOPMENT OF WO<sub>3</sub>-TiO<sub>2</sub> NANOTUBE ARRAYS  
FOR WATER ELECTROLYSIS**

**by**

**LAI CHIN WEI**

**Thesis submitted in fulfillment of the requirements  
for the degree of  
Doctor of Philosophy**

**MARCH 2013**

## ACKNOWLEDGEMENT

First and foremost, I would like to thank Universiti Sains Malaysia (USM), especially School of Materials and Mineral Resources Engineering (SMMRE) for offering an opportunity and providing a conducive research environment with sufficient facilities to complete my research project. I would also like to acknowledge the USM Fellowship and Research University Postgraduate Research Grant Scheme for providing financial support.

I would also like to express my sincerest gratitude to my supervisor, Assoc. Prof. Dr. Srimala Sreekantan for extending continuous encouragement, support and guidance throughout my doctoral study. Her inspired suggestions and assistance were instrumental to the progress of my research. This thesis would not have completed without her constant guidance.

On top of that, my sincere gratefulness to the Dean of SMMRE, Prof. Hanafi b. Ismail and former Dean, Prof. Ahmad Fauzi b. Mohd Noor for their concern and invaluable support throughout my doctoral study. Special thank to all the academic and technical staff of SMMRE for their advices and assistance. I would also like to thank my postgraduate colleagues for helping me during my experimental work.

Furthermore, I would like to express my gratitude and appreciation to all my friends for their supports throughout the years. They had encouraged me towards achieving my goals in this project. The most important support has come from my beloved parents and my family members, who have always stood beside me and have supported me during every step of my life.

Last but not least, I would like to thank everyone who was important to the successful realization of thesis, as well as expressing my apology that I could not mention personally one by one. Thank you very much.

## TABLE OF CONTENTS

	<b>Page</b>
<b>ACKNOWLEDGEMENT</b>	ii
<b>TABLE OF CONTENTS</b>	iii
<b>LIST OF TABLES</b>	viii
<b>LIST OF FIGURES</b>	x
<b>LIST OF ABBREVIATIONS</b>	xx
<b>LIST OF SYMBOLS</b>	xxi
<b>LIST OF PUBLICATIONS</b>	xxii
<b>ABSTRAK</b>	xxvii
<b>ABSTRACT</b>	xxix
<b>CHAPTER 1 INTRODUCTION</b>	
1.1 Introduction	1
1.2 Problem statement	4
1.3 Research objectives	7
1.4 Scope of research	7
1.5 Outline of Dissertation	10
<b>CHAPTER 2 LITERATURE REVIEW</b>	
2.1 Introduction	11
2.2 Historical overview of PEC water splitting	12

2.3	Basic principle of PEC water splitting	14
2.4	Material selection for PEC water splitting	17
2.5	TiO <sub>2</sub> photocatalyst for PEC water splitting	19
2.6	TiO <sub>2</sub> nanotube arrays	21
	2.6.1 Formation of TiO <sub>2</sub> nanotube arrays	22
	2.6.2 The four synthesis generation of TiO <sub>2</sub> nanotubes	23
	2.6.3 Mechanism of formation of TiO <sub>2</sub> nanotubes	24
2.7	Tuning the photocatalytic of TiO <sub>2</sub> into the visible light region	28
2.8	WO <sub>3</sub> -incorporated TiO <sub>2</sub> photocatalyst	34
	2.8.1 Structural and electronic properties of WO <sub>3</sub> -TiO <sub>2</sub> photocatalyst	35
2.9	Preparation of WO <sub>3</sub> -TiO <sub>2</sub> photocatalyst	39
	2.9.1 Hydrothermal synthesis	39
	2.9.2 Sol-gel technique	42
	2.9.3 Wet impregnation technique	43
	2.9.4 Other techniques	45
	2.9.5 Radio frequency sputtering technique	49
2.10	Water photoelectrolysis	51

### **CHAPTER 3 MATERIALS AND METHODOLOGY**

3.1	Introduction	55
3.2	Raw materials and chemicals selection	56
3.3	Experimental procedure	57
	3.3.1 Ti foil preparation	57
	3.3.2 Electrolyte preparation	58

3.3.3 Anodization process	58
3.3.4 Cleaning of the as-anodized TiO <sub>2</sub> foil	59
3.3.5 Preparation of WO <sub>3</sub> -TiO <sub>2</sub> nanotubes (RF sputtering)	59
3.3.6 Preparation of WO <sub>3</sub> -TiO <sub>2</sub> nanotubes (wet impregnation)	59
3.3.7 Heat treatment process	60
3.3.8 PEC water splitting cell testing	61
3.4 Design of experiment	62
3.4.1 Anodic growth of TiO <sub>2</sub> nanotubes	63
3.4.2 Incorporation of WO <sub>3</sub> into TiO <sub>2</sub> nanotubes	65
3.4.2.1 RF sputtering technique	66
3.4.2.2 Wet impregnation technique	67
3.4.3 PEC water splitting performance evaluation	68
3.5 Characterization techniques	69
3.5.1 Field Emission Scanning Electron Microscopy (FESEM)	70
3.5.2 Energy Dispersion X-ray (EDX)	71
3.5.3 Transmission Electron Microscope (TEM)	71
3.5.4 X-Ray Diffraction (XRD)	72
3.5.5 Raman Spectroscopy	73
3.5.6 X-ray Photoelectron Spectroscopy (XPS)	74
3.5.7 Photoluminescence (PL) Spectroscopy	75

## **CHAPTER 4 RESULTS AND DISCUSSIONS**

4.1 Introduction	76
4.2 Anodization of Ti in glycerol	77

4.3	Anodization of Ti in pure ethylene glycol	81
4.4	Anodization of Ti in ethylene glycol containing water	82
4.5	Effect of H <sub>2</sub> O <sub>2</sub> in the electrolyte on the anodic oxide formed	84
4.6	Effect of H <sub>2</sub> O <sub>2</sub> addition compared with water addition	87
4.7	Effect of anodization time	89
4.8	Dimensional control of TiO <sub>2</sub> nanotube with continuous H <sub>2</sub> O <sub>2</sub> addition	91
4.9	Effect of different cleaning methods	96
4.10	Effect of fluoride content	100
4.11	Effects of anodization applied voltage	103
4.12	Effect of anodization temperature	105
4.13	Effect of thermal treatment on anodized TiO <sub>2</sub> nanotubes	110
4.14	PEC water splitting performance evaluation	114
4.14.1	Effect of organic additive in PEC electrolyte	114
4.14.2	Effect of different anodic TiO <sub>2</sub> morphologies	119
4.14.3	Effect of different aspect ratio TiO <sub>2</sub> nanotubes	123
4.14.4	Effect of crystallization of TiO <sub>2</sub> nanotubes	126
4.15	Incorporation of WO <sub>3</sub> into TiO <sub>2</sub> nanotubes	131
4.15.1	Introduction	131
4.15.2	Effect of RF sputtering times (RF sputtering)	132
4.15.3	Effect of RF sputtering powers (RF sputtering)	149
4.15.4	Effect of heat treatment on WO <sub>3</sub> -TiO <sub>2</sub> nanotubes	159
4.15.5	Effect of molarity of APT solution (wet impregnation)	170
4.15.6	Effect of soaking time in APT solution (wet impregnation)	183

## **CHAPTER 5 CONCLUSION AND SUGGESTIONS**

5.1 Conclusion 193

5.2 Suggestions and recommendation 196

**REFERENCES** 198

## LIST OF TABLES

		<b>Page</b>
Table 2.1	Summary of the works reported on the different cationic-loaded TiO <sub>2</sub> photocatalyst.	32
Table 2.2	Summary of the works reported on the recent approach to synthesis WO <sub>3</sub> -TiO <sub>2</sub> photocatalyst via hydrothermal technique.	41
Table 2.3	Summary of the works reported on the recent approach to synthesis WO <sub>3</sub> -TiO <sub>2</sub> photocatalyst via sol-gel technique.	44
Table 2.4	Summary of the works reported on the recent approach to synthesis WO <sub>3</sub> -TiO <sub>2</sub> photocatalyst via wet impregnation technique.	46
Table 2.5	Summary of the works reported on the recent approach to synthesis WO <sub>3</sub> -TiO <sub>2</sub> photocatalyst via other techniques	47
Table 2.6	Summary of WO <sub>3</sub> -TiO <sub>2</sub> photocatalyst in water photoelectrolysis application.	54
Table 3.1	List of raw materials and chemicals used to fabricate TiO <sub>2</sub> nanotubes and WO <sub>3</sub> -TiO <sub>2</sub> nanotubes as well as chemical used in PEC studies with its function and manufacturer.	56
Table 3.2	The parameters investigated on the geometrical features of the anodic growth of TiO <sub>2</sub> nanotubes.	65
Table 3.3	The parameters investigated in RF sputtering to produce WO <sub>3</sub> -TiO <sub>2</sub> nanotubes and constant parameter used in this study.	66
Table 3.4	The parameters investigated in wet impregnation to produce WO <sub>3</sub> -TiO <sub>2</sub> nanotubes and constant parameter used in this study.	67
Table 3.5	The parameters investigated in PEC water splitting studies.	69
Table 4.1	Experimental conditions used to synthesize TiO <sub>2</sub> nanotubes with the addition of H <sub>2</sub> O <sub>2</sub> at different interval times.	92
Table 4.2	Experimental conditions used to achieve different microstructures and geometries in the anodic TiO <sub>2</sub> samples.	120
Table 4.3	Summary of the PEC water splitting performance for TiO <sub>2</sub> photoanode with different surface morphologies.	123



Table 4.4	Experimental conditions used to achieve different aspect ratio of TiO <sub>2</sub> nanotubes in ethylene glycol containing 5 wt% of H <sub>2</sub> O <sub>2</sub> and 5 wt% of NH <sub>4</sub> F for 1 h.	124
Table 4.5	Summary of the PEC water splitting performance of TiO <sub>2</sub> nanotubes with different aspect ratios and geometric surface area factors.	125
Table 4.6	Experimental conditions used to achieve TiO <sub>2</sub> nanotubes with different crystal structures.	126
Table 4.7	Average at% of TiO <sub>2</sub> and WO <sub>3</sub> -TiO <sub>2</sub> nanotubes at different deposition times obtained by EDX analysis.	134
Table 4.8	Average at% of pure TiO <sub>2</sub> and WO <sub>3</sub> -TiO <sub>2</sub> nanotubes at different sputter powers obtained by EDX analysis.	152
Table 4.9	Summary of the PEC water splitting performance for WO <sub>3</sub> -TiO <sub>2</sub> nanotubes subjected different sputtering powers.	158
Table 4.10	Average at% of WO <sub>3</sub> -TiO <sub>2</sub> nanotubes at different annealing temperatures obtained by EDX analysis.	161
Table 4.11	Summary of the PEC water splitting performance for WO <sub>3</sub> -TiO <sub>2</sub> nanotubes subjected different heat treatment temperatures.	169
Table 4.12	Average at% of pure TiO <sub>2</sub> and WO <sub>3</sub> -TiO <sub>2</sub> nanotubes produced at different molarities of APT solution obtained from EDX analysis.	172
Table 4.13	Summary of PEC water splitting performance for WO <sub>3</sub> -TiO <sub>2</sub> nanotubes soaked in different molarities of APT solution.	181
Table 4.14	Average at% of pure TiO <sub>2</sub> and WO <sub>3</sub> -TiO <sub>2</sub> nanotubes at different soaking times obtained by EDX analysis.	183
Table 4.15	Summary of PEC water splitting performance of WO <sub>3</sub> -TiO <sub>2</sub> nanotubes soaked at different times in APT solution.	189

## LIST OF FIGURES

		<b>Page</b>
Figure 2.1	Basic principle of the overall water splitting reaction on a semiconductor photocatalyst (Leung <i>et al.</i> , 2010).	14
Figure 2.2	Energy diagram for an n-type semiconductor-metal in photoelectrolysis cell (Neelkanth <i>et al.</i> , 2009).	16
Figure 2.3	Electronic structure of different semiconductors and the relative position of their band edge vs. some key redox potentials (Grätzel, 2001).	18
Figure 2.4	SEM images of (a) cross sectional image of TiO <sub>2</sub> nanotubes, inset is the image with higher magnification, (b) top view of TiO <sub>2</sub> nanotubes, and (c) bottom of TiO <sub>2</sub> nanotubes (Zhang <i>et al.</i> , 2010).	21
Figure 2.5	(a) Typical experimental setup of anodization system and (b) schematic diagram of the typical structure of TiO <sub>2</sub> nanotubes after anodization process (Macak <i>et al.</i> , 2007).	22
Figure 2.6	Schematic diagram of porous TiO <sub>2</sub> nanotube formation: (A) oxide growth to maximal thickness (B) burst of oxide by the formation of crystallites (pore formation), (C) immediate repassivation of pore tips, (D) burst of repassivated oxide, and (E) dissolution of the formed oxide and second repassivation. (Choi <i>et al.</i> , 2004).	25
Figure 2.7	Schematic diagram of the evolution of a nanotube arrays at constant anodization voltage: (a) oxide layer formation, (b) pit formation on the oxide layer, (c) growth of the pit into scallop shaped pores, (d) metallic part between the pores undergoes oxidation and field assisted dissolution, and (e) fully developed nanotube array with a corresponding top view (Mor <i>et al.</i> , 2006).	26
Figure 2.8	Schematic diagram (left column) and SEM sequence (top-views – middle column, cross-sections – right column) of different stages of the TiO <sub>2</sub> nanotubes layer formation. Anodization stopped after (a) 0 min, (b) 3 min, (c) 10 min, (d) 30 min, (e) 1 h from reaching 20 V in water/glycerol/0.27 M NH <sub>4</sub> F after potential ramp from 0 to 20 V with a sweep rate of 250 mV/s (Schmuki <i>et al.</i> , 2007).	27

Figure 2.9	Band structure of a cationic-loaded on wide band gap of semiconductor photocatalyst with visible light response. (Navarro Yerga <i>et al.</i> , 2009).	31
Figure 2.10	1 x 2 supercell model of a TiO <sub>2</sub> (101) anatase surface with 3 O-Ti-O layers. Atoms labeling for the substitutional W positions: 5s, pentacoordinated surface site; 6s, hexacoordinated surface site; 6u, subsurface hexacoordinated (up) site; and 6d, hexacoordinated subsurface (down) site. [Atom colors: Ti, grey; and O, red] (Marquez <i>et al.</i> , 2011)	38
Figure 2.11	Supercell models of W-doped TiO <sub>2</sub> (101) anatase surface showing the defects introduced to achieve charge compensation: (a) model with two W atoms incorporating a V <sub>Ti</sub> site (light blue sphere) and (b) model with one W atom and an extra O included. The models show the most relevant bond distances (in Å). Top: side view; Bottom: top view. [Atom colors: Ti, grey; O, red; W, ochre] (Marquez <i>et al.</i> , 2011)	38
Figure 2.12	Proposed mechanism for the formation process of the W loaded anatase nanoparticles and the two types of W species during the hydrothermal treatment of phosphotungstate-titania nanocomposites (Kim <i>et al.</i> , 2009).	40
Figure 2.13	The scheme of RF-sputtering chamber (Ghodselahi <i>et al.</i> , 2008).	49
Figure 2.14	Schematic diagram of the separation of photo-generated electrons and holes on the WO <sub>3</sub> -TiO <sub>2</sub> photocatalyst interface (Meng <i>et al.</i> 2011).	52
Figure 3.1	Schematic diagram of the anodization experiment set-up.	58
Figure 3.2	Annealing profile of TiO <sub>2</sub> nanotubes and WO <sub>3</sub> -TiO <sub>2</sub> nanotubes at 400 °C in argon atmosphere.	60
Figure 3.3	Experimental set-up of H <sub>2</sub> generation by the PEC water splitting process.	62
Figure 3.4	Flow chart of overall process in this research study.	63
Figure 3.5	Methodology flow chart for anodization process.	64
Figure 3.6	Methodology flow chart in PEC water splitting performance evaluation.	68

Figure 4.1	FESEM images of TiO <sub>2</sub> nanotubes fabricated at 30 V in 1M of glycerol electrolyte containing 5 wt% NH <sub>4</sub> F for 30 min. (a) Top view, and (b) cross-sectional view.	78
Figure 4.2	(a) Current density against time plot for anodized Ti foils at 30 V for 30 min in 1M glycerol electrolyte containing 5 wt% NH <sub>4</sub> F, (b) schematic illustration to explain the formation of oxide layer (region I), and (c) schematic illustration to explain the field-assisted dissolution and chemical dissolution of the barrier layer (region II and region III ).	79
Figure 4.3	XRD pattern of TiO <sub>2</sub> nanotubes (a) as-anodized and (b) annealed at 400°C in argon atmosphere for the sample formed in 1M of glycerol electrolyte containing 5 wt% NH <sub>4</sub> F at 30 V for 30 min [Ti=Titanium; A=Anatase].	80
Figure 4.4	FESEM images of the TiO <sub>2</sub> nanotubes produced in the ethylene glycol containing 5 wt% of NH <sub>4</sub> F at 60 V for 1 h, (a) Top view and (b) cross sectional view.	82
Figure 4.5	FESEM images of the TiO <sub>2</sub> nanotubes produced in ethylene glycol containing NH <sub>4</sub> F and water under optimized condition (a) Side view 20K magnification and the inset is 3K magnification, and (b) Top view of the peeled surface of TiO <sub>2</sub> foil and the inset is bottom part of peeled nanotube arrays.	83
Figure 4.6	Top view (left) and cross-sectional view (right) of FESEM images of TiO <sub>2</sub> nanotubes obtained using different wt% of H <sub>2</sub> O <sub>2</sub> in ethylene glycol containing 5 wt% NH <sub>4</sub> F for 1 h at 60 V are shown. The wt% of H <sub>2</sub> O <sub>2</sub> are as follows: (a) 1 wt%; (b) 3 wt%; (c) 5 wt%; and (d) 10 wt%.	85
Figure 4.7	FESEM image of Ti foil anodized for 5 min at 60 V in ethylene glycol containing 5 wt% of NH <sub>4</sub> F: (a) 5 wt% of water; and (b) 5 wt% of H <sub>2</sub> O <sub>2</sub> .	88
Figure 4.8	Current density-time behavior during anodization of Ti in two different electrolytes at 60 V: (a) ethylene glycol containing 5 wt% of NH <sub>4</sub> F and 5 wt% H <sub>2</sub> O <sub>2</sub> ; and (b) ethylene glycol containing 5 wt% of NH <sub>4</sub> F and 5 wt% of water.	88
Figure 4.9	FESEM images of TiO <sub>2</sub> nanotubes obtained in ethylene glycol containing 5 wt% NH <sub>4</sub> F and 5 wt% H <sub>2</sub> O <sub>2</sub> at different anodization times: (a) 0.5 min; (b) 1 min; (c) 30 min; (d) 120 min; and (e) 180 min.	89

Figure 4.10	Variation of TiO <sub>2</sub> nanotube array lengths as a function of anodization time: (a) TiO <sub>2</sub> nanotube obtained in ethylene glycol containing 5 wt% NH <sub>4</sub> F and 5 wt% H <sub>2</sub> O <sub>2</sub> ; and (b) TiO <sub>2</sub> nanotubes obtained in ethylene glycol containing 5 wt% NH <sub>4</sub> F and 5 wt% H <sub>2</sub> O.	90
Figure 4.11	FESEM images of TiO <sub>2</sub> nanotube arrays anodized in ethylene glycol containing 5 wt% NH <sub>4</sub> F and 5 wt% H <sub>2</sub> O <sub>2</sub> at 60 V for 1 h: Samples (a) A, (b) B, (c) C and (d) D; TEM images of TiO <sub>2</sub> nanotubes: Samples (e) A, (f) B, (g) C, and (h) D.	94
Figure 4.12	Schematic illustration explaining the formation of highly ordered TiO <sub>2</sub> nanotubes: (a) sample C, and sample D (Macak <i>et al.</i> , 2007).	95
Figure 4.13	FESEM images of TiO <sub>2</sub> nanotubes obtained via different cleaning methods after the anodization process; (a) ultrasonically cleaned in distilled water for 1 min and subsequently dried under flowing N <sub>2</sub> gas and (b) cleaned by hot rinsing at 90 °C using distilled water for 1 min and subsequently dried under flowing N <sub>2</sub> gas.	97
Figure 4.14	FESEM images of TiO <sub>2</sub> nanotubes obtained via chemical etching using 2% HF after anodization for (a) 10, (b) 15, (c) 20, and (d) 60 s.	98
Figure 4.15	FESEM images of TiO <sub>2</sub> nanotubes obtained via ultrasonic cleaning using acetone after anodization for (a) 1, (b) 2, and (c) 10 min.	99
Figure 4.16	FESEM images of the TiO <sub>2</sub> nanotubes synthesized with different NH <sub>4</sub> F concentrations in ethylene glycol solution and 5 wt% H <sub>2</sub> O <sub>2</sub> electrolyte for 60 min at 60 V. (a) 1.67 wt%, (b) 3.33 wt%, (c) 6.67 wt%, and (d) 8.33 wt%.	102
Figure 4.17	Current density as a function of NH <sub>4</sub> F concentration in ethylene glycol containing 5 wt% H <sub>2</sub> O <sub>2</sub> at 60 V for 1 h.	103
Figure 4.18	FESEM images of TiO <sub>2</sub> nanotubes obtained with different anodization voltage for 1 h in ethylene glycol containing 5 wt% NH <sub>4</sub> F and 5 wt% of H <sub>2</sub> O <sub>2</sub> electrolyte, (a) 10 V, (b) 20 V, (c) 30 V, (d) 40 V, (e) 50 V, and (f) 70V.	105
Figure 4.19	FESEM images of TiO <sub>2</sub> nanotubes fabricated at (a) 10 °C, (b) 20 °C, (c) 40 °C, (d) 60 °C, and (e) 80 °C in ethylene glycol containing 5 wt% H <sub>2</sub> O <sub>2</sub> and 5 wt% NH <sub>4</sub> F anodized at 60 V for 1 h.	107

Figure 4.20	The effect of anodization temperature on the (a) length, (b) pore diameter and (c) wall thickness of the TiO <sub>2</sub> nanotubes anodized in ethylene glycol containing 5 wt% of NH <sub>4</sub> F and 5 wt% of H <sub>2</sub> O <sub>2</sub> at 60 V for 1 h.	108
Figure 4.21	Current density as function of anodization temperatures.	109
Figure 4.22	Color of electrolyte obtained upon Ti foil anodized in ethylene glycol containing 5 wt% of NH <sub>4</sub> F and 5 wt% of H <sub>2</sub> O <sub>2</sub> (a) before anodization process, (b) at 10 °C, (c) at room temperature, and (d) at 60 °C.	109
Figure 4.23	Schematic illustration explaining the diffusion rate of ionic species at metal-oxide layers above the Ti foil, (a) Stage 1 (cool condition), (b) room temperature (27 °C), and (c) Stage 2 (warm condition) (Macak <i>et al.</i> , 2007).	110
Figure 4.24	FESEM micrographs of TiO <sub>2</sub> nanotubes annealed at different temperatures for 4 h in argon atmosphere, (a) as-anodized sample, (b) 200°C, (c) 300°C, (d) 500°C, (e) 600°C and (f) 700°C.	111
Figure 4.25	XRD patterns of the TiO <sub>2</sub> nanotubes annealed at different temperatures, (a) as-anodized, (b) 200°C, (c) 300°C, (d) 400°C, (e) 500°C, (f) 600°C , and (g) 700°C [A=Anatase; T=Titanium; R=Rutile].	113
Figure 4.26	The j <sub>p</sub> -V characteristics of TiO <sub>2</sub> nanotubes photoanode in 1M KOH solution with (a) 1 wt% of ethylene glycol, (b) 5 wt% of ethylene glycol, (c) 10 wt% of ethylene glycol, and (d) without ethylene glycol under illumination.	115
Figure 4.27	A potentiostatic plot of TiO <sub>2</sub> nanotubes in 1M KOH solution with (a) 1 wt% of ethylene glycol, (b) 5 wt% of ethylene glycol, (c) 10 wt% of ethylene glycol, and (d) without ethylene glycol under illumination.	117
Figure 4.28	The η curves of TiO <sub>2</sub> nanotubes in 1M KOH solution with (a) 1 wt% of ethylene glycol, (b) 5 wt% of ethylene glycol, (c) 10 wt% of ethylene glycol, and (d) without ethylene glycol under illumination.	118
Figure 4.29	H <sub>2</sub> evolution of TiO <sub>2</sub> nanotubes in 1M KOH solution with (a) 1 wt% of ethylene glycol, (b) 5 wt% of ethylene glycol, (c) 10 wt% of ethylene glycol, and (d) without ethylene glycol under illumination for 1 h.	119
Figure 4.30	The j <sub>p</sub> -V characteristic curves of TiO <sub>2</sub> photoanode with different surface morphologies.	120

Figure 4.31	A Potentiostatic plot of $j_p$ for $\text{TiO}_2$ photoanode with different surface morphologies under interrupted illumination.	122
Figure 4.32	The $j_p$ -V characteristic curves of $\text{TiO}_2$ nanotubes with different aspect ratios and geometric surface area factors.	125
Figure 4.33	The $j_p$ -V characteristic curves of $\text{TiO}_2$ nanotubes with different crystal structures.	127
Figure 4.34	The potentiostatic plot of $\text{TiO}_2$ nanotubes with different crystal structures.	129
Figure 4.35	The $\eta$ curves of $\text{TiO}_2$ nanotubes with different crystal structures.	130
Figure 4.36	$\text{H}_2$ evolution of the $\text{TiO}_2$ nanotubes with different crystal structures under illumination for 1 h.	130
Figure 4.37	Top-view of FESEM images of $\text{TiO}_2$ nanotubes loaded with $\text{WO}_3$ and sputtered for (a) 0.5, (b) 1, (c) 3, (d) 5, and (e) 10 min.	132
Figure 4.38	(a) TEM image of $\text{WO}_3$ - $\text{TiO}_2$ nanotubes sputtered for 0.5 min; and its mapping image of (b) W element, (c) Ti element, (d) O element, as well as TEM image of $\text{WO}_3$ - $\text{TiO}_2$ nanotubes sputtered for 10 min in magnification of (e) 50000X and (f) 125000X.	135
Figure 4.39	XRD patterns of (a) pure $\text{TiO}_2$ , and the $\text{TiO}_2$ nanotubes loaded with $\text{WO}_3$ and sputtered for (b) 0.5, (c) 1, (d) 3, (e) 5, and (f) 10 min [A = Anatase, T = Titanium, W= Tungsten trioxide].	136
Figure 4.40	The Raman spectra: (a) pure $\text{TiO}_2$ nanotubes, and $\text{WO}_3$ - $\text{TiO}_2$ nanotubes sputtered for (b) 0.5 min and (c) 10 min [A = Anatase, W= Tungsten trioxide].	138
Figure 4.41	XPS spectra of $\text{Ti}2p$ region: (a) pure $\text{TiO}_2$ nanotubes and $\text{WO}_3$ - $\text{TiO}_2$ nanotubes sputtered for (b) 0.5 min and (c) 10 min.	139
Figure 4.42	XPS spectra of $\text{O}1s$ region: (a) pure $\text{TiO}_2$ nanotubes and $\text{WO}_3$ - $\text{TiO}_2$ nanotubes sputtered for (b) 0.5 min and (c) 10 min.	140
Figure 4.43	XPS spectra of $\text{W}4d$ region: (a) pure $\text{TiO}_2$ nanotubes and $\text{WO}_3$ - $\text{TiO}_2$ nanotubes sputtered for (b) 0.5 min and (c) 10 min.	141

Figure 4.44	XPS spectra of W4f region: (a) pure TiO <sub>2</sub> nanotubes and WO <sub>3</sub> -TiO <sub>2</sub> nanotubes sputtered for (b) 0.5 min and (c) 10 min.	142
Figure 4.45	XPS spectra of the C1s region: (a) pure TiO <sub>2</sub> nanotubes, and WO <sub>3</sub> -TiO <sub>2</sub> nanotubes sputtered for (b) 0.5 and (c) 10 min.	142
Figure 4.46	Photoluminescence (PL) spectra of (a) pure TiO <sub>2</sub> and TiO <sub>2</sub> nanotubes incorporated with WO <sub>3</sub> and sputtered for (b) 10 min and (c) 0.5 min.	143
Figure 4.47	The j <sub>p</sub> -V characteristic curves of TiO <sub>2</sub> and WO <sub>3</sub> -TiO <sub>2</sub> nanotubes at different sputtering times: (a) WO <sub>3</sub> -loaded nanotubes sputtered for 0.5 and (b) 1 min; (c) pure TiO <sub>2</sub> nanotubes, and (d) WO <sub>3</sub> -loaded nanotubes sputtered for 3, (e) 5, and (f) 10 min.	145
Figure 4.48	The potentiostatic plot of sample (a) WO <sub>3</sub> -loaded nanotubes sputtered for 0.5 and (b) 1 min; (c) pure TiO <sub>2</sub> nanotubes, and (d) WO <sub>3</sub> -loaded nanotubes sputtered for 3, (e) 5, and (f) 10 min.	146
Figure 4.49	The η curves of TiO <sub>2</sub> nanotubes at different sputtering times: (a) WO <sub>3</sub> -loaded nanotubes sputtered for 0.5 and (b) 1 min; (c) pure TiO <sub>2</sub> nanotubes and (d) WO <sub>3</sub> -loaded nanotubes sputtered for 3, (e) 5, and (f) 10 min.	146
Figure 4.50	H <sub>2</sub> evolution of (a) WO <sub>3</sub> -loaded nanotubes sputtered for 0.5 and (b) 1 min; (c) pure TiO <sub>2</sub> nanotube, and (d) WO <sub>3</sub> -loaded nanotubes sputtered for 3, (e) 5, and (f) 10 min.	147
Figure 4.51	Schematic diagram of the photo-induced electrons trapped by WO <sub>3</sub> under solar illumination.	148
Figure 4.52	FESEM top view image of different sputtering powers for (a) 50 W, (b) 100 W, (c) 180 W, (d) 200 W, and (e) 250 W on the TiO <sub>2</sub> nanotubes, inset image with cross sectional view.	150
Figure 4.53	TEM images of different sputtering powers for (a) pure TiO <sub>2</sub> nanotubes (b) 50 W, (c) 180 W, and (d) 250 W on the TiO <sub>2</sub> nanotubes.	151
Figure 4.54	Schematic illustration explaining the effect of different RF sputtering powers on the TiO <sub>2</sub> nanotubes.	151
Figure 4.55	Raman spectra of (a) TiO <sub>2</sub> nanotubes, (b) sample sputtered for 50 W, and (c) sample sputtered for 200 W	153
Figure 4.56	PL spectra of (a) pure TiO <sub>2</sub> nanotubes, (b) sample sputtered for 50 W, and (c) sample sputtered for 200 W.	154



Figure 4.57	XPS of the W4d region: (a) TiO <sub>2</sub> nanotubes, (b) sample sputtered for 50 W, and (c) sample sputtered for 200 W.	155
Figure 4.58	XPS of the W4f region: (a) TiO <sub>2</sub> nanotubes, (b) sample sputtered for 50 W, and (c) sample sputtered for 200 W.	155
Figure 4.59	The j <sub>p</sub> -V characteristic curves of the different RF sputtering powers of the WO <sub>3</sub> -TiO <sub>2</sub> nanotubes under light condition, (a) 50 W, (b) 100 W, (c) 180 W, (d) 200 W, (e) pure TiO <sub>2</sub> nanotubes, and (f) 250 W.	156
Figure 4.60	Potentiostatic plot of WO <sub>3</sub> -TiO <sub>2</sub> nanotubes, (a) 50 W, (b) 100 W, (c) 180 W, (d) 200 W, (e) pure TiO <sub>2</sub> nanotube, and (f) 250 W under interrupted light illumination.	158
Figure 4.61	FESEM micrographs of WO <sub>3</sub> -TiO <sub>2</sub> nanotubes annealed at different temperatures for 4 h in argon atmosphere, (a) as-anodized sample, (b) 200 °C, (c) 300 °C, (d) 500 °C, (e) 600 °C and (f) 700 °C.	160
Figure 4.62	XRD patterns of the WO <sub>3</sub> -TiO <sub>2</sub> nanotubes annealed at different temperatures, (a) as-anodized, (b) 200 °C, (c) 300 °C, (d) 400 °C, (e) 500 °C, (f) 600 °C, and (g) 700 °C [A=Anatase; T=Titanium; R=Rutile].	162
Figure 4.63	Raman spectra of WO <sub>3</sub> -TiO <sub>2</sub> with different annealing temperatures, (a) 400 °C, (b) 500 °C and (c) 600 °C [A=Anatase; R=Rutile; W=Tungsten Trioxide].	164
Figure 4.64	XPS survey spectra for WO <sub>3</sub> -loaded TiO <sub>2</sub> nanotubes, (a) as-anodized, (b) annealed at 400 °C and (c) annealed at 600 °C.	165
Figure 4.65	The W4d peak for WO <sub>3</sub> -loaded TiO <sub>2</sub> nanotubes, (a) as-anodized, (b) annealed at 400 °C and (c) annealed at 600 °C.	165
Figure 4.66	The PL spectra of WO <sub>3</sub> -loaded TiO <sub>2</sub> nanotubes with different annealing temperatures, (a) 400 °C (b) 500 °C (c) 600 °C.	166
Figure 4.67	The j <sub>p</sub> -V characteristic curves of WO <sub>3</sub> -TiO <sub>2</sub> nanotubes subjected to different temperatures, (a) 400°C, (b) 500°C, (c) 600°C, (d) 300°C, (e) 700°C, (f) 200°C, and (g) as-anodized.	167
Figure 4.68	Potentiostatic plot of WO <sub>3</sub> -TiO <sub>2</sub> nanotubes subjected to different temperatures, (a) 400 °C, (b) 500 °C, (c) 600 °C, (d) 300 °C, (e) 700 °C, (f) 200 °C, and (g) as-anodized.	168
Figure 4.69	Top-view FESEM images of WO <sub>3</sub> -TiO <sub>2</sub> nanotubes soaked in (a) 0.1, (b) 0.3, (c) 0.5, (d) 1, and (e) 5 mM APT solution for 1 h.	171

Figure 4.70	TEM images of (a) pure TiO <sub>2</sub> and WO <sub>3</sub> -TiO <sub>2</sub> nanotubes soaked in (b) 0.3 and (c) 5 mM APT solution for 1h.	172
Figure 4.71	XRD diffraction patterns of (a) pure TiO <sub>2</sub> and WO <sub>3</sub> -TiO <sub>2</sub> nanotubes soaked in (b) 0.1, (c) 0.3, (d) 0.5, (e) 1, and (f) 5 mM APT solution for 1h.	174
Figure 4.72	PL spectra of (a) pure TiO <sub>2</sub> and WO <sub>3</sub> -TiO <sub>2</sub> nanotubes soaked (b) 0.3 and (c) 5 mM APT solution.	176
Figure 4.73	XPS spectra of the Ti2p region of (a) pure TiO <sub>2</sub> and WO <sub>3</sub> -TiO <sub>2</sub> nanotubes soaked in (b) 0.3 and (c) 5 mM APT solution.	177
Figure 4.74	XPS spectra of the O1s region of (a) pure TiO <sub>2</sub> and WO <sub>3</sub> -TiO <sub>2</sub> nanotubes soaked in (b) 0.3 and (c) 5 mM APT solution.	178
Figure 4.75	XPS spectra of the C1s region of (a) pure TiO <sub>2</sub> and WO <sub>3</sub> -TiO <sub>2</sub> nanotubes soaked in (b) 0.3 and (c) 5 mM APT solution.	179
Figure 4.76	XPS spectra of the W4d region for (a) pure TiO <sub>2</sub> and WO <sub>3</sub> -TiO <sub>2</sub> nanotubes soaked in (b) 0.3 and (c) 5 mM APT solution.	180
Figure 4.77	XPS spectra of the W4f region of (a) pure TiO <sub>2</sub> and WO <sub>3</sub> -TiO <sub>2</sub> nanotubes soaked in (b) 0.3 and (c) 5 mM APT solution.	180
Figure 4.78	The j <sub>p</sub> -V characteristic curves of WO <sub>3</sub> -TiO <sub>2</sub> nanotubes soaked at different molarities of APT solution: (a) 0.3 mM, (b) 0.1 mM, (c) 0.5 mM, (d) pure TiO <sub>2</sub> nanotubes, (e) 1 mM, and (f) 5 mM.	181
Figure 4.79	The potentiostatic plot of WO <sub>3</sub> -TiO <sub>2</sub> nanotubes soaked at different molarities of APT solution: (a) 0.3 mM, (b) 0.1 mM, (c) 0.5 mM, (d) pure TiO <sub>2</sub> nanotubes, (e) 1 mM, and (f) 5 mM.	182
Figure 4.80	FESEM images of WO <sub>3</sub> -TiO <sub>2</sub> nanotubes soaked for (a) 2, (b) 3, (c) 4, and (d) 5 h in 0.3 mM APT solution.	183
Figure 4.81	XRD diffraction patterns of (a) pure TiO <sub>2</sub> and WO <sub>3</sub> -TiO <sub>2</sub> nanotubes soaked for (b) 2, (c) 3, (d) 4, and (e) 5 h.	184
Figure 4.82	Raman spectra of (a) pure TiO <sub>2</sub> and WO <sub>3</sub> -TiO <sub>2</sub> nanotubes soaked for (b) 2 and (c) 5 h.	186
Figure 4.83	XPS spectra of the W4d region for (a) pure TiO <sub>2</sub> and WO <sub>3</sub> -TiO <sub>2</sub> nanotubes soaked for (b) 2 and (c) 5 h.	187
Figure 4.84	XPS spectra of the W4f region for (a) pure TiO <sub>2</sub> and WO <sub>3</sub> -TiO <sub>2</sub> nanotubes soaked for (b) 2 and (c) 5 h.	187

Figure 4.85	PL spectra: (a) pure TiO <sub>2</sub> and WO <sub>3</sub> -TiO <sub>2</sub> nanotubes soaked for (b) 2 and (c) 5 h.	188
Figure 4.86	The j <sub>p</sub> -V characteristic curves of (a) WO <sub>3</sub> -TiO <sub>2</sub> nanotubes soaked for 2 and (b) 3 h and (c) pure TiO <sub>2</sub> and WO <sub>3</sub> -TiO <sub>2</sub> nanotubes soaked for (d) 4 and (e) 5 h.	189
Figure 4.87	Potentiostatic plot of (a) WO <sub>3</sub> -TiO <sub>2</sub> nanotubes soaked for 2 and (b) 3 h and (c) pure TiO <sub>2</sub> and WO <sub>3</sub> -TiO <sub>2</sub> nanotubes soaked for (d) 4 and (e) 5 h.	190
Figure 4.88	H <sub>2</sub> evolution under light illumination of (a) WO <sub>3</sub> -TiO <sub>2</sub> nanotubes soaked for 2 and (b) 3 h and (c) pure TiO <sub>2</sub> and WO <sub>3</sub> -TiO <sub>2</sub> nanotubes soaked for (d) 4 and (e) 5 h.	191
Figure 4.89	Schematic diagram of the photo-induced electrons trapped by WO <sub>3</sub> . These photo-induced electrons were then transported rapidly from the nanotube walls to the Ti substrate for photocurrent generation.	192

## LIST OF ABBREVIATIONS

AR	Aspect ratio
APT	Ammonium paratungstate
C <sub>B</sub>	Conduction band
CBD	Chemical bath deposition
DFT	Density functional theory
DI	Deionized water
EDX	Energy dispersive X-ray spectroscopy
E <sub>B</sub>	Band-gap energy
E <sub>F</sub>	Fermi level
EG	Ethylene glycol
EISA	Evaporation-induced self-assembly
FESEM	Field emission scanning electron microscopy
G	Geometric surface area factor
GLAD	Glancing angle deposition
LSP	Linear sweep potential
MB	Methyl blue
MO	Methyl orange
NHE	Normal hydrogen electrode
PEC	Photoelectrochemical
PL	Photoluminescence
RF	Radio Frequency
RT	Room temperature
SCE	Saturated calomel electrode
SEM	Scanning electron microscope
TEM	Transmission electron microscopy
UV	Ultraviolet
V <sub>B</sub>	Valence band
V <sub>fb</sub>	Flat band potential
V <sub>oc</sub>	Open-circuit potential
XPS	X-ray photoelectron spectroscopy
XRD	X-ray diffraction

## LIST OF SYMBOLS

$h\nu$	Photon energy
$\text{\AA}$	Angstrom
atm	Standard atmosphere
at%	Atomic percentage
cm	Centimeter
$e^-$	Electron
h	Hour
$h^+$	Hole
eV	Electronvolt
$\Delta G^\circ$	Gibbs free energy
$I_0$	Power density of the incident light
$j_p$	Photocurrent density
kHz	Kilohertz
M	Molar
mA	Milliampere
mL	Milliliter
mm	Millimeter
mM	Millimolar
min	Minute
nm	Nanometer
s	Second
$\mu\text{m}$	Micrometer
V	Voltage
$V_{oc}$	Open-circuit voltage
W	Watt
wt%	Weight percentage
$\lambda$	Radiation wavelength
$\eta$	Photoconversion efficiency
$\theta$	Diffraction angle
$^\circ\text{C}$	Degree Celsius
$\phi$	Work function

## LIST OF PUBLICATIONS

### Patents:

1. Sreekantan S., Arifin Z.A., Lockman Z., **Lai C.W.**, Hazan R. and Saharudin K.A. (2012). An apparatus and method for rapid rate of titanium dioxide (TiO<sub>2</sub>) nanotubes arrays formation, International application published under the Patent Cooperation Treaty (PCT), *International Patent Publication. Number: WO/2012/026799.*
2. Sreekantan S., Arifin Z.A., Lockman Z., **Lai C.W.**, Hazan R. and Saharudin K.A. (2012). An apparatus and method for rapid rate of titanium dioxide (TiO<sub>2</sub>) nanotubes arrays formation, *Intellectual Property Corporation of Malaysia, Filing Number: PI 201004009.*

### Published papers in refereed journals:

1. Sreekantan S. and **Lai C.W.** (2010). Study on the formation and photocatalytic activity of titanate nanotubes synthesized via hydrothermal method. *Journal of Alloys and Compounds* 490, p. 436 – 442.
2. **Lai C.W.** and Sreekantan S. (2010). Comparison of long and short titania nanotubes on the photocatalytic activity. *Malaysian Journal of Microscopy* 6, p. 48 – 52.
3. Sreekantan S., **Lai C.W.** and Lockman Z. (2011). Extremely fast growth rate of TiO<sub>2</sub> nanotube arrays in electrochemical bath containing H<sub>2</sub>O<sub>2</sub>. *Journal of the Electrochemical Society* 158, p. C397 – C402.
4. Sreekantan S., Hazan R., Saharudin K.A, **Lai C.W.** and Mat I. (2011). Formation of high aspect ratio TiO<sub>2</sub> nanotube arrays by anodization of Ti Foil in organic solution. *Sains Malaysiana* 40, p. 227 – 230.
5. Sreekantan S., Saharudin K.A. and **Lai C.W.** (2011). Formation of TiO<sub>2</sub> nanotubes via anodization and potential applications for photocatalysts, biomedical materials, and photoelectrochemical cell. *IOP Conference Series: Materials Science and Engineering* 21, p. 012002.
6. **Lai C.W.** and Sreekantan S. (2011). Effect of applied potential on the formation of self-organized TiO<sub>2</sub> nanotubes and its photoelectrochemical response. *Journal of Nanomaterials* 2011, p. 142463.

7. **Lai C.W.** and Sreekantan S. (2012). Photoelectrochemical properties of TiO<sub>2</sub> nanotube arrays: Effect of electrolyte pH and annealing temperature. *Journal of Experimental Nanoscience*, In press, DOI: 10.1080/17458080.2011.654276.
8. Sreekantan S., **Lai C.W.**, E P.S. and Krengvirat W. (2012). Nanotubular transition metal oxide for hydrogen production. *Advanced Materials Research* 364, p. 484 – 499.
9. **Lai C.W.** and Sreekantan S. (2012). Visible light photoelectrochemical performance of W-loaded TiO<sub>2</sub> nanotube arrays: Structural properties. *Journal of Nanoscience and Nanotechnology* 12, p. 3170 – 3174.
10. **Lai C.W.**, Sreekantan S. and Lockman Z. (2012). Photoelectrochemical behaviour of uniform growth TiO<sub>2</sub> nanotubes via bubble blowing synthesized in ethylene glycol with H<sub>2</sub>O<sub>2</sub>. *Journal of Nanoscience and Nanotechnology*, 12, p. 4057 – 4066.
11. **Lai C.W.** and Sreekantan S. (2012). Photoelectrochemical performance of smooth TiO<sub>2</sub> nanotube arrays: Effect of anodization temperature and cleaning methods. *International Journal of Photoenergy* 2012, p. 356943.
12. **Lai C.W.** and Sreekantan S. (2012). Comparison of photocatalytic and photoelectrochemical behavior of TiO<sub>2</sub> nanotubes prepared by different organic electrolyte. *Optoelectronics and Advanced Materials – Rapid Communications* 6, p. 82 – 86.
13. **Lai C.W.** and Sreekantan S. (2012). WO<sub>3</sub> deposited TiO<sub>2</sub> nanotube arrays by thermal evaporation method for effective photocatalytic activity. *Journal of Engineering Science* 8, p. 37 – 48.
14. **Lai C.W.**, Sreekantan S. and E P.S. (2012). Effect of radio frequency sputtering power on W-TiO<sub>2</sub> nanotubes to improve photoelectrochemical performance. *Journal of Material Research* 27, p. 1695 – 1704.
15. **Lai C.W.** and Sreekantan S. (2012). Dimensional control of TiO<sub>2</sub> nanotube arrays with H<sub>2</sub>O<sub>2</sub> content for high photoelectrochemical water splitting performance. *Micro & Nano Letters* 7, p. 443 – 447.
16. **Lai C.W.**, Sreekantan S., E P.S. and Krengvirat W. (2012). Preparation and photoelectrochemical characterization of WO<sub>3</sub>-loaded TiO<sub>2</sub> nanotube arrays via radio frequency sputtering. *Electrochimica Acta* 77, p. 128 – 136.

17. **Lai C.W.** and Sreekantan S. (2012). Photoelectrochemical response studies of W deposited TiO<sub>2</sub> nanotubes via thermal evaporation technique. *Journal of Experimental Nanoscience*. In press, DOI: 10.1080/17458080.2012.705439.
18. **Lai C.W.** and Sreekantan S. (2012). Optimized sputtering power to incorporate WO<sub>3</sub> into C-TiO<sub>2</sub> nanotubes for highly visible photoresponse performance. *NANO* 7, p. 1250051.
19. **Lai C.W.** and Sreekantan S. (2012). Higher water splitting hydrogen generation rate for single crystalline anatase phase of TiO<sub>2</sub> nanotube arrays. *The European Physical Journal - Applied Physic* 59, p. 20403.
20. **Lai C.W.** and Sreekantan S. (2013). TiO<sub>2</sub> nanotubes arrays: Improved photoelectrochemical response by adding optimum amount of ethylene glycol in KOH electrolyte. *Nanoscience and Nanotechnology Letters* 5, p. 57 – 62.
21. **Lai C.W.** and Sreekantan S. (2013). Study of WO<sub>3</sub> incorporated C-TiO<sub>2</sub> nanotubes for efficient visible light driven water splitting performance. *Journal of Alloys and Compounds* 547, p. 43 – 50.
22. **Lai C.W.** and Sreekantan S. (2013). Discovery of WO<sub>3</sub>/TiO<sub>2</sub> nanostructure transformation by controlling content of NH<sub>4</sub>F to enhance photoelectrochemical response. *Advanced Material Research* 620, p. 173 – 178.
23. **Lai C.W.** and Sreekantan S. (2013). Incorporation of WO<sub>3</sub> species into TiO<sub>2</sub> nanotubes via wet impregnation and their water-splitting performance. *Electrochimica Acta* 87, p. 294 – 302.
24. **Lai C.W.** and Sreekantan S. (2013). Preparation of hybrid WO<sub>3</sub>-TiO<sub>2</sub> nanotube photoelectrode using anodization and wet impregnation: Improved water-splitting hydrogen generation performance. *International Journal of Hydrogen Energy* 38, p. 2156 – 2166.
25. **Lai C.W.** and Sreekantan S. (2013). Fabrication of WO<sub>3</sub> nanostructures by anodization for visible-light driven water splitting and photodegradation of methyl orange. *Materials Science in Semiconductor Processing*, In press, DOI: 10.1016/j.mssp.2012.10.007.
26. **Lai C.W.** and Sreekantan S. (2013). Heat treatment effects of WO<sub>3</sub>-loaded TiO<sub>2</sub> nanotubes with enhanced water splitting hydrogen generation. *Materials Science in Semiconductor Processing*, In press, DOI: 10.1016/j.mssp.2013.02.002



27. **Lai C.W.** and Sreekantan S. (2013). The photoelectrochemical response of various surface morphologies of titanium anodic oxide films. *Journal of Engineering Science*, In press, Accepted for publication

**Published papers in conference proceedings:**

1. Sreekantan S., Lockman Z., Hazan R., Saharudin K.A. and **Lai C.W.** (2009). Formation of high aspect ratio TiO<sub>2</sub> nanotube arrays by anodization of Ti foil in organic solution, *Proceeding of Nanotech Malaysia 2009*, 27–29<sup>th</sup> Oct 2009, Kuala Lumpur Convention Centre, Kuala Lumpur Malaysia.
2. Sreekantan S., Hazan R., Saharudin K.A. and **Lai C.W.** (2009). TiO<sub>2</sub> nanotube arrays: An ultimate solution for green environment, *Proceeding of the 2<sup>nd</sup> AUN/Seed-Net Regional Conference on Materials Engineering: Material For Changing World*, 19–20<sup>th</sup> Nov 2009, The Tide Resort, Thailand.
3. **Lai C.W.** and Sreekantan S. (2009). Decoration of TiO<sub>2</sub> nanotubes structure with WO<sub>3</sub> for effective photocatalytic activity, *Proceeding of Nanomaterials Synthesis & Characterization Conference NMSC 2009*, 3–4<sup>th</sup> Nov 2009, Palace of the Golden Horses, Seri Kembangan, Selangor, Malaysia.
4. **Lai C.W.** and Sreekantan S. (2009). Comparison of the long and short TiO<sub>2</sub> nanotubes on the photocatalytic activity, *Proceeding of the 18<sup>th</sup> Scientific Conference of Electron Microscopy Society of Malaysia*, 15–17<sup>th</sup> Dec 2009, Palace of the Golden Horses, Seri Kembangan, Selangor, Malaysia.
5. **Lai C.W.** and Sreekantan S. (2010). Effect of fluoride content and cleaning agent on the formation of self organized TiO<sub>2</sub> nanotube arrays, *Proceeding of International Conference on X-Rays & Related Techniques in Research & Industry*, 9–10<sup>th</sup> Jun 2010, Aseania Resort Langkawi, Malaysia.
6. Sreekantan S., Hazan R., Saharudin K.A., **Lai C.W.** and Mat I. (2009). Studies on formation of TiO<sub>2</sub> nanotube arrays with various anodization parameters and photocatalytic application, *Proceeding of Nanomaterials Synthesis & Characterization Conference NMSC 2009*, 3–4<sup>th</sup> Nov 2009, Palace of the Golden Horses, Seri Kembangan, Selangor, Malaysia.
7. Sreekantan S., Saharudin K.A. and **Lai C.W.** (2011). Formation of TiO<sub>2</sub> nanotube via anodization and its potential application, *Proceeding of International Symposium on Global Multidisciplinary Engineering 2011*, 24–25<sup>th</sup> Jan 2011, Nagaoka University of Technology, Japan.

8. Sreekantan S., **Lai C.W.**, E P.S. and Hamzah N.A. (2011). Anodic growth of nanostructured TiO<sub>2</sub> and WO<sub>3</sub>: Morphology and photoelectrochemical response, *Proceeding of International Symposium On Material Science Engineering And Energy Technology*, 30<sup>th</sup> June–1<sup>st</sup> Jul 2011, Faculty of Science and Technology Thammasat University (Rangsit Campus), Thailand.
10. Sreekantan S., Saharudin K.A. and **Lai C.W.** (2011). NANOpurifier - A sustainable way of destroying contaminants in air and water, *Proceeding of Joint Research Seminar USM-NUT 2011*, 17<sup>th</sup> Oct 2011, Institute For Research In Molecular Medicine (INFORMM) Universiti Sains Malaysia, Malaysia.
11. **Lai C.W.** and Sreekantan S. (2011). Enhanced photoelectrochemical response using TiO<sub>2</sub> nanotubes by adding ethylene glycol as organic additive, *Proceeding of 20<sup>th</sup> Scientific Conference of the Electron Microscopy Society of Malaysia*, 20–22<sup>nd</sup> Dec 2011, Permaisuri Resort, Port Dickson, Malaysia.
12. **Lai C.W.** and Sreekantan S. (2012). The photoelectrochemical response of various surface morphologies of titanium anodic oxide films, *Proceeding of the Asian International Conference on Materials, Minerals, and Polymer 2012*, 23–23<sup>rd</sup> Mar 2012, Vistana Hotel Penang, Malaysia.
13. **Lai C.W.** and Sreekantan S. (2012). Discovery of WO<sub>3</sub>/TiO<sub>2</sub> nanostructure transformation by controlling content of NH<sub>4</sub>F to enhance photoelectrochemical response, *Proceeding of International Conference on X-Rays & Related Techniques in Research & Industry*, 3–5<sup>th</sup> Jul 2012, Vistana Hotel, Penang, Malaysia.

#### **Awards:**

1. Gold Medal & Romanian Best Innovation Award,  
E P.S., **Lai C.W.** and Sreekantan S. (2011). *World Invention Awards London 2011 at the British Invention Show (BIS) held at Alexandra Palace*, United Kingdom on 19–22<sup>nd</sup> Oct 2011, for project entitles: Hybrid Transition Oxide Nanotube – Bridge to sustainable economy.
2. Gold Medal,  
Sreekantan S., Arifin Z.A., **Lai C.W.**, Saharudin K.A. and Krengvirat W. (2011). *Korea International Women's Invention Exposition 2011*, Seoul, Korea, hosted by the Korean Intellectual Property Office (KIPO) and organized by the Korea Women Inventors Association (KWIA) on 4–7<sup>th</sup> May 2011, for project entitles: Nanopurifier- A sustainable way of destroying contaminants in air and water.

# PEMBANGUNAN SUSUNAN TIUBNANO WO<sub>3</sub>-TiO<sub>2</sub> DALAM ELEKTROLISIS AIR

## ABSTRAK

Penjanaan hidrogen solar melalui elektrolisis air adalah sasaran utama untuk pembangunan ekonomi hidrogen secara lestari bagi sistem tenaga masa depan. Pembentukan TiO<sub>2</sub> tiubnano yang bebas daripada kelompok adalah penting dalam aplikasi elektrolisis air supaya mencapai kecekapan yang tinggi. Kajian terperinci terhadap kesan komposisi elektrolit, masa penganodan, keupayaan elektrik, suhu penganodan dan suhu penyepuhlindapan telah dilaksanakan bagi mengawal susunan dan geometri tiubnano. Susunan tiubnano TiO<sub>2</sub> yang mempunyai permukaan dinding licin dan nisbah aspek yang tinggi telah berjaya disintesis dalam glikol etilena yang mengandungi 5 wt% NH<sub>4</sub>F dan 5 wt% H<sub>2</sub>O<sub>2</sub> melalui kaedah penganodan pada 60 V selama 1 jam. H<sub>2</sub>O<sub>2</sub> digunakan sebagai pembekal oksigen untuk meningkatkan kadar pengoksidaan dan seterusnya meningkatkan kadar pembentukan tiubnano dalam kajian ini. Sehubungan dengan itu, didapati bahawa penambahan hidrogen peroksida ke dalam elektrolit dalam selang masa 10 min menghasilkan tiubnano yang lebih panjang (~ 13 µm) dengan diameter ~ 140 nm. Usaha berterusan telah dilaksanakan bagi meningkatkan lagi prestasi elektrolisis air dengan mendeposisi WO<sub>3</sub> pada TiO<sub>2</sub> tiubnano melalui teknik pemercikan RF dan pengisitepuan basah. WO<sub>3</sub>-TiO<sub>2</sub> tiubnano yang dipercik dengan daya pemercikan 50 W selama 0.5 min serta disepuhlindap pada 400 °C telah menunjukkan foto-arus sebanyak 2.4 mA/cm<sup>2</sup> yang tinggi dengan kecekapan penukaran foto sebanyak 6.2 %. Peningkatan prestasi sebanyak dua kali ganda telah dicatatkan berbanding dengan TiO<sub>2</sub> tiubnano yang asal. Sebaliknya, TiO<sub>2</sub> tiubnano yang dicelupkan dalam 0.3 mM larutan APT selama 1

jam menunjukkan foto-arus sebanyak  $2.1 \text{ mA/cm}^2$  dengan kecekapan penukaran foto sebanyak 5.1 %.  $\text{WO}_3\text{-TiO}_2$  tiubnano yang dihasilkan melalui teknik pemercikan RF mencatatkan prestasi elektrolisis air yang lebih tinggi berbanding dengan teknik pengisitepuan basah. Penemuan ini menunjukkan bahawa pengenapan  $\text{W}^{6+}$  spesies dalam kekisi  $\text{TiO}_2$  dengan tenaga kinetik yang tinggi (pemercikan RF) mencapai prestasi elektrolisis air yang lebih baik berbanding dengan proses resapan daripada  $\text{W}^{6+}$  spesies ke dalam kekisi  $\text{TiO}_2$  (pengisitepuan basah). Kehadiran unsur W di bawah 1 at% dalam  $\text{TiO}_2$  menunjukkan peningkatan foto-arus dan kecekapan penukaran foto kerana ia akan bertindak sebagai pengantara yang berkesan untuk memerangkap elektron dan mengurangkan rekombinasi elektron-lohong. Sebaliknya, kandungan  $\text{WO}_3$  yang berlebihan akan membentuk akumulasi pada permukaan tiubnano dan mengakibatkan prestasi elektrolisis air menjadi rendah kerana lapisan asing ini akan bertindak sebagai pusat rekombinasi elektron-lohong.

# DEVELOPMENT OF WO<sub>3</sub>-TiO<sub>2</sub> NANOTUBE ARRAYS FOR WATER ELECTROLYSIS

## ABSTRACT

Solar hydrogen generation from water electrolysis is a key target for the development of sustainable hydrogen economy for future energy system. The formation of self-organized TiO<sub>2</sub> nanotubes without bundling is essential for high efficiency in photoelectrochemical (PEC) water electrolysis application. Comprehensive investigations on different parameters, such as composition of electrolyte, anodization time, anodization voltage, anodization temperature and heat treatment temperature were conducted in order to control the specific architecture of nanotubes. Highly ordered and smooth TiO<sub>2</sub> nanotubes were successfully synthesized through anodization of Ti foil in ethylene glycol containing 5 wt% of NH<sub>4</sub>F and 5 wt% of H<sub>2</sub>O<sub>2</sub> at 60 V for 1 h. In this study, H<sub>2</sub>O<sub>2</sub> was used as oxygen provider to increase the oxidation rate for synthesizing nanotubes at a rapid rate. It was found that addition of H<sub>2</sub>O<sub>2</sub> at 10 min intervals formed longer nanotubes (~ 13 μm) with larger pore diameter (~ 140 nm). Continuous efforts have been exerted to further improve the PEC water splitting performance by incorporating an optimum content of WO<sub>3</sub> into TiO<sub>2</sub> nanotubes using RF sputtering and wet impregnation techniques. It was found that TiO<sub>2</sub> nanotubes sputtered at 50 W for 0.5 min and subsequently heat treated at 400 °C demonstrated a maximum photocurrent density of ~ 2.4 mA/cm<sup>2</sup> with photoconversion efficiency ~ 6.2 %. This performance was approximately two times higher than the pure TiO<sub>2</sub> nanotubes. On the other hand, TiO<sub>2</sub> nanotubes that dipped into the 0.3 mM ammonium paratungstate (APT) solution for 1 h showed photocurrent density of ~ 2.1 mA/cm<sup>2</sup> with photoconversion

efficiency of ~ 5.1 %. The  $\text{WO}_3\text{-TiO}_2$  nanotubes prepared by RF sputtering exhibited higher PEC water splitting performance than that of wet impregnation. These findings deduced that  $\text{W}^{6+}$  species incorporated within  $\text{TiO}_2$  lattice by high kinetic energy process (RF sputtering) exhibited better PEC performance than the diffusion of  $\text{W}^{6+}$  species into  $\text{TiO}_2$  lattice (wet impregnation). The presence of W element below 1 at% in  $\text{TiO}_2$  showed an improvement of photocurrent density and photoconversion efficiency because it acted as an effective mediator to trap the photo-induced electrons and minimize the recombination of charge carriers. By contrast, excessive content of  $\text{WO}_3$  loading on the wall surface of  $\text{TiO}_2$  nanotubes resulted in poor PEC water splitting performance because it formed independent layers that acted as recombination centers for the charge carriers.

## CHAPTER 1

### INTRODUCTION

#### 1.1 Introduction

At present, modern society is habituated to a high degree of mobility, fast communication and daily comfort, all of which require considerable energy input (Grimes *et al.*, 2008). These energy inputs largely consist of fossil fuel, which in turn, after combustion, contributes to the greenhouse gases and increases the carbon footprint in the earth's atmosphere. The addition of greenhouse gases are said to be largely responsible for increasing extreme climate conditions, which have wrought havoc on many nations across the world in the past several years (Ohi, 2005; Yu and Chen, 2009). Many scientists aware that the extraction and combustion of fossil fuels will release significant amount of greenhouse gases to the atmosphere and this is a major threat to the environment because it causes land damage, smog, acid rain and atmospheric changes (Bockris, 2002; Ghicov and Schmuki, 2009). Environmental damage and atmospheric changes may soon alter the weather and climate patterns of the earth, resulting in grave problems of all its inhabitants.

One of the steps taken by many countries to aid the earth and minimizing environmental problems is applying sustainable development. It seems that sustainable development is a strategic goal of modern society reflecting contemporary demand for economic, social, political and environmental development (Turner, 1999; Aroutiounian *et al.*, 2005; Jefferson, 2006). Therefore, executing research for generating green and renewable energy resource has been the passion for scientists, which can provide us energy in sustainable manner. The finding of alternative clean energy source is crucial in leading a high quality of life, which is in harmony with nature (Kreuter and Hofmann, 1998; Marsen *et al.*, 2007).

To date, hydrogen ( $H_2$ ) has been established as a potential future energy carrier and possibly the best substitute for fossil fuel to secure the future supply of a clean and sustainable energy (Funk, 2001; Tromp *et al.*, 2003; Ewan and Allen, 2005). The novel feature of  $H_2$  is that it can be produced from water using solar energy, which are readily available and renewable resources without carbon emission (Tryk *et al.* 2000; Bak *et al.* 2002; Grätzel, 2003; Mahajan *et al.*, 2008; Maeda *et al.*, 2010). However, the future will certainly not be based on a simple replacement of fossil fuels by  $H_2$  fuel as a commercial source of energy.  $H_2$  must be produced and made available at cheaper cost for everyone to utilize it without creating any imbalance in global ecology. Among viable renewable  $H_2$  production approaches, the use of photoelectrochemical (PEC) water splitting system has become one of the most promising methods and has high potential in the  $H_2$  economy to secure the future supply of clean and recyclable  $H_2$  energy (Grätzel, 2003; Paulose *et al.*, 2006; Liu *et al.*, 2011).

In order to bring  $H_2$  to the point of commercial readiness and establish  $H_2$  economy, substantial research on the development of semiconductor for water splitting process using solar energy has been developed lately (Leung *et al.*, 2010; Kubacka *et al.*, 2012). Although a number of semiconductor have been reported to be active photocatalysts for the overall water splitting reaction, most of them only function under ultraviolet (UV) light ( $\lambda < 400$  nm) owing to the wide band gap energy. Since nearly half of the solar energy incident on the earth's surface falls in the visible region ( $400 < \lambda < 800$  nm), the efficient use of visible light is essential for generating  $H_2$  gas through water splitting process (Ni *et al.*, 2007; Ahn *et al.*, 2007; Shon *et al.*, 2008; Fujishima *et al.*, 2008). Unfortunately, overall PEC water splitting using visible light is difficult to achieve due to the band level of the semiconductor is



rather difficult to be tuned to visible region (Kitano *et al.*, 2007; Abe *et al.*, 2011; Tong *et al.*, 2012). To date, no known semiconductor has been discovered that simultaneously meets all the criteria required for economical H<sub>2</sub> production (Grimes *et al.*, 2008; Kubacka *et al.*, 2012).

In fact, a suitable candidate as a photoelectrode for H<sub>2</sub> production must have three basic criteria as shown below (Grimes and Mor, 2009):

i. Stability:

The semiconductor must be photochemically stable in aqueous solution, in which it will not be photocorroded during the photoelectrolysis process.

ii. Band gap:

The semiconductor must have a band gap about 1.7-2.0 eV as considering the overpotential losses and energy required for water splitting process.

iii. Energy Level:

For spontaneous water splitting process, the oxidation and reduction potential must lie between the valence and conduction band edges of the semiconductor.

In the field of photocatalysis today, titanium dioxide (TiO<sub>2</sub>) has emerged as the leading candidate as an efficient photoelectrode in PEC water splitting system because of its unique characteristics, such as high stability against corrosion, non-toxicity, strong oxidation ability, good photocatalytic property, self-cleaning property, and ready availability (Ho *et al.*, 2006; Grimes, 2007; Roy *et al.*, 2011). However, an obvious hindrance to the widespread use of TiO<sub>2</sub> as a photoelectrode is its poor visible light response resulting from its large band gap (3.2 eV on the anatase polymorph) and the rapid recombination of photo-induced electron/hole pairs (Ahn *et al.*, 2007; Hathway *et al.*, 2009; Leung *et al.*, 2010). Several researchers have

argued that the visible light absorption of  $\text{TiO}_2$  can be improved in the past few years. This can be done by coupling  $\text{TiO}_2$  with another semiconductor, which will lead to additional electronic state in the band-gap, which in turn affect a change in the optical, electronic and functionality of  $\text{TiO}_2$ . (Mohapatra *et al.*, 2008; Shen *et al.*, 2008; Zhang *et al.*, 2010; Nah *et al.*, 2010; Bang and Kamat, 2010; Costi *et al.*, 2010; Das *et al.*, 2011). Other than poor response of  $\text{TiO}_2$  to visible light, the multi-component semiconductors are complex materials. Making intuitive guesses on their properties are more or less impossible, and a focused research on the area is a very challenging task.

To split water under visible light, the incorporation of  $\text{WO}_3$  into  $\text{TiO}_2$  photocatalyst has received much more attention in the literatures recently due to the interesting and unique features of the resultant binary oxide system (Fernandez-Garcia *et al.*, 2005; Higashimoto *et al.*, 2008; Sajjad *et al.*, 2010; Wang *et al.*, 2011). In this manner, coupling  $\text{TiO}_2$  with small band-gap of  $\text{WO}_3$  that possess different redox energy level for their valence band and conduction band, which provides another attractive approach to achieve more efficient charge separation under visible light (Barreca *et al.*, 2011). A hybrid of  $\text{WO}_3$ - $\text{TiO}_2$  nanotubes, acting as a photoelectrode in PEC water splitting system has been developed in our study recently. Results suggest that the hybrid  $\text{WO}_3$ - $\text{TiO}_2$  nanotubes demonstrate significant advantages of promoting the separation of electron/hole pairs and responsive to the visible light in PEC water splitting system.

## **1.2 Problem statement**

The exceptional chemical and physical properties of  $\text{TiO}_2$  have been long recognized since the discovery of water photoelectrolysis on  $\text{TiO}_2$  by Fujishima and

Honda in 1972. To date, one-dimensional (1D) structure of well-aligned TiO<sub>2</sub> nanotubes by a simple electrochemical oxidation reaction of a Ti substrate under a specific set of environment conditions have been widely reported (Mishra *et al.*, 2003; Raja *et al.*, 2005; Mor *et al.*, 2006; Paulose *et al.* 2006). However, TiO<sub>2</sub> nanotubes are still far from becoming a potential candidate for PEC water splitting system. Bundling problem (disorder arrangement of nanotube arrays) and weak adherence of the nanotube arrays on Ti substrate remains as a great challenge. In addition, poor visible light absorption and rapid recombination of charge carriers limit the widespread use of TiO<sub>2</sub> nanotubes (Ahn *et al.*, 2007; Zhang *et al.*, 2010; Márquez *et al.*, 2011; Kubacka *et al.*, 2012). Thus, in order to produce high efficient PEC water splitting system using TiO<sub>2</sub> nanotubes as a photoelectrode is challenging unless several issues have pointed out are addressed.

One of the ways to improve the PEC water splitting performance of TiO<sub>2</sub> is creating 1D nanotubular structures with desired length, pore diameter and wall thickness through anodization method. Anodization is the most feasible method due to its ability to create self-organized anodic oxides in the form of nanotubular structures with almost perfect vertical alignment. Moreover, anodization is relatively simple; it can be adopted for large-scale industrial production (Todorova *et al.*, 2008; Yasuda *et al.*, 2007; Roy *et al.*, 2011). However, in getting the right dimensions and morphologies, a controlled synthesis procedure for the production of well-aligned 1D TiO<sub>2</sub> nanotubes must be investigated and optimized. Generally, highly ordered TiO<sub>2</sub> nanotubes result in undesirable bundling problems, which significantly decrease the photoconversion efficiencies in the PEC water splitting system (Zhu *et al.*, 2007; Kim *et al.*, 2008; Baker and Kamat, 2009). Therefore, in the present study, considerable efforts have been devoted to the synthesis of stable (good

photoresponse and high chemical stability), clean (bundle-free), and highly ordered TiO<sub>2</sub> nanotubes that could increase the PEC water splitting performance.

To resolve the above listed problems of the TiO<sub>2</sub>, continuous efforts have been conducted by coupling a narrow band-gap semiconductor with TiO<sub>2</sub> in order to enhance the charge separation efficiency (Mohapatra *et al.*, 2008; Shen *et al.*, 2008; Costi *et al.*, 2010; Das *et al.*, 2011). In this case, the narrow band-gap semiconductor must fulfill several basic requirements for better charge separation efficiency, such as the conduction band of narrow band-gap semiconductor should be more positive than that of the TiO<sub>2</sub>, responsive to visible light and photo-corrosion free condition (Navarro Yerga *et al.*, 2009).

In the present study, WO<sub>3</sub> was selected as a suitable semiconductor to be coupled with TiO<sub>2</sub> nanotubes due to suitable band edge position relative to TiO<sub>2</sub>, strong reversible field-aided ion intercalation, and exhibit higher surface acidity to absorb more ionic species on the surface of TiO<sub>2</sub>. In this manner, conduction band electrons from TiO<sub>2</sub> can be injected to the WO<sub>3</sub> due to the internal electrostatic field from the interpretation of inter-band state (Nah *et al.*, 2008; Benoit *et al.*, 2009; Gong *et al.*, 2011). Besides, WO<sub>3</sub> offers relatively small band gap energy (2.5 eV to 2.8 eV) and exhibit strong absorption within solar spectrum (Abe *et al.*, 2011; Song *et al.*, 2011). Another important reason for using hybrid WO<sub>3</sub>-TiO<sub>2</sub> as photoelectrode in PEC water splitting system is because of long term inertness to chemical environment and resilience to photocorrosion over a wide pH range in aqueous solution under evolving oxygen conditions (Fernandez-Garcia *et al.*, 2005; Kim *et al.*, 2009; Márquez *et al.*, 2011).

### 1.3 Research objectives

The objectives of this study are listed as follow:-

- i. To study the effect of electrochemical parameters on the formation of TiO<sub>2</sub> nanotubes (e.g., composition of electrolyte, time, temperature, cleaning methods, heat treatment temperature) by anodization method.
- ii. To study the effect of geometry (e.g., aspect ratio, surface morphology, crystal structure) of the anodized TiO<sub>2</sub> nanotubes on the PEC characteristic studies.
- iii. To study the formation of WO<sub>3</sub>-TiO<sub>2</sub> nanotubes via RF sputtering technique (e.g., sputtering time, sputtering power) and wet impregnation technique (e.g., molarity of precursor, soaking time).
- iv. To study the PEC characteristic studies (e.g., photocurrent density, photoresponse, photoconversion efficiency and amount of H<sub>2</sub> generation) of WO<sub>3</sub>-TiO<sub>2</sub> nanotubes as compared to the pure TiO<sub>2</sub> nanotubes.

### 1.4 Scope of research

Anodization is the most feasible method for synthesis of TiO<sub>2</sub> nanostructures because it yields anodic oxides with nanotubular structures in a well-aligned manner. Thus, TiO<sub>2</sub> nanotubes with controlled dimensional features and free from bundling or clustering are essential prior to WO<sub>3</sub> incorporation. Therefore, in the present study, the formation of TiO<sub>2</sub> nanotubes in organic electrolyte (ethylene glycol) was investigated. Then, the possibility of forming TiO<sub>2</sub> nanotubes at faster rate in the presence of hydrogen peroxide (H<sub>2</sub>O<sub>2</sub>) in ethylene glycol electrolyte was investigated in detail. In addition, the effect of the composition of electrolyte, anodization time, applied voltage, anodization temperature and heat treatment temperature on the nanotube geometry (e.g., length, pore diameter and wall thickness) were studied in

order to understand the optimum architecture of nanotube arrays for high efficient PEC water splitting performance. Unlike other works,  $\text{H}_2\text{O}_2$  is used in here instead of water as oxygen provider to accelerate the field assisted oxidation and thus high aspect ratio nanotubes could be achieved. Furthermore, the use of  $\text{H}_2\text{O}_2$  in ethylene glycol electrolyte was found to be beneficial in addressing bundling and adherence problems of nanotube arrays. The growth mechanism of  $\text{TiO}_2$  nanotubes in such electrolyte was investigated too.

Many studies highlighted the coupling mechanism between  $\text{WO}_3$  and  $\text{TiO}_2$  to facilitate better charge carrier separation and visible light response (Higashimoto *et al.*, 2008; Das *et al.*, 2011; Gong *et al.*, 2011). However, most of these studies involved  $\text{WO}_3$ - $\text{TiO}_2$  photocatalysts in the form of particles/spheres or thin films, which do not possess high enough surface area for photon absorption (Yan and Zhou, 2011; Kubacka *et al.*, 2012). Moreover, most scholars mainly focused on the photodegradation of organic pollutants rather than the PEC water splitting application. Therefore, detail studies regarding the relationship of the  $\text{WO}_3$  content incorporated into  $\text{TiO}_2$  nanotubes for PEC water splitting performance has been established in this work. To the best of our knowledge, incorporation of  $\text{WO}_3$  into 1D  $\text{TiO}_2$  nanotubes using radio frequency (RF) sputtering technique to improve PEC water splitting performance is not available. Meanwhile, little information is known regarding the formation of  $\text{WO}_3$ - $\text{TiO}_2$  nanotubes photoelectrode through wet impregnation technique, especially in PEC water splitting application. Thus, a comprehensive study was conducted to optimize RF sputtering parameters (e.g., sputtering time and sputtering power) and wet impregnation parameters (e.g., molarity of precursor and soaking time) to obtain the desired  $\text{WO}_3$ - $\text{TiO}_2$  nanotubes, resulting in best PEC water splitting performance.

The surface and cross-sectional morphologies of the anodized Ti foils was viewed by field emission scanning electron microscopy (FESEM) and transmission electron microscopy (TEM). The elemental analysis was determined with energy dispersion X-ray (EDX). Besides, X-ray diffraction (XRD) was used to investigate the crystallinity and phase transition of the sample. In addition, Raman analysis was used to obtain the vibrational information specific to the chemical bonds and symmetrical of molecules in the sample. Meanwhile, high sensitive surface analysis of X-ray photoelectron spectroscopy (XPS) was selected to identify and quantify the elemental composition and oxidation state from the sample surface. Then, the fundamental information on the properties of the energy levels lying within the band gap as well as the efficiency of charge carrier trapping, immigration and transfer was investigating using photoluminescence (PL) measurement.

The PEC water splitting performance of the samples were characterized using a three-electrodes PEC cell with TiO<sub>2</sub> nanotubes as the working photoelectrode, a platinum rod as the counter electrode, and a saturated calomel electrode (SCE) as the reference electrode. The electrolyte used in the PEC cell consisted of 1 M potassium hydroxide (KOH) aqueous solution. All of the three electrodes were connected to a potentiostat ( $\mu$ Autolab III), and the current and voltage were measured. A 150 W Xenon arc lamp solar simulator (Zolix LSP-X150) with an intensity of 800 W/m<sup>2</sup> was used to produce a largely continuous and uniform spectrum. The photocurrent densities of the samples were measured. Next, the responsiveness of the samples to the interrupted illumination and the H<sub>2</sub> evolution measurements were studied. The evolved H<sub>2</sub> gas was collected using a reverted burette.

## **1.5 Outline of dissertation**

This dissertation is organized in five chapters consecutively. In chapter 1, the introduction of this research work, research objectives, problem statement, the scope of research as well as dissertation overview are presented. Chapter 2 provides an overview of the principles, and the research progress of solar H<sub>2</sub> generation production via the water splitting reaction using TiO<sub>2</sub> nanotubes. In addition, chapter 2 comprises literature review on the WO<sub>3</sub> incorporated TiO<sub>2</sub> photocatalyst using different approaches. The specifications of the raw materials, research methodology, and the characterizations employed in this research work are described in chapter 3. The results of characterizations and the discussions are presented in chapter 4. Chapter 5 summarizes the conclusion of the study as well as several suggestions and recommendations for the future work. Such finding will aid in building the fundamentals of TiO<sub>2</sub> nanotubes modification with WO<sub>3</sub> in the development of H<sub>2</sub> fuel cell for sustainable energy system.



## CHAPTER 2

### LITERATURE REVIEW

#### 2.1 Introduction

Nowadays, public concern about the environment, climate change and limited fossil fuel resources have given rise to the urgent need of fostering development in the area of renewable energies, which are inexhaustible and non-polluting (Turner, 1999; Ohi, 2005; Jefferson, 2006). The production of H<sub>2</sub> gas is one of the most promising prospects for efficient renewable resources (Funk, 2001; Bockris, 2002; Tromp *et al.*, 2003; Ewan and Allen, 2005). To bring H<sub>2</sub> to the point of commercial readiness and viability in terms of performance and cost, substantial research on the development of n-type semiconductor for PEC water splitting process using solar energy is necessary (Tryk *et al.* 2000; Bak *et al.* 2002).

Recent studies have indicated that TiO<sub>2</sub> has emerged as the leading candidate for PEC water splitting cell because of its low cost, non-toxicity, self-cleaning property, ready availability and strong photocatalytic activity and stability against photocorrosion (Raja *et al.*, 2005; Ho *et al.*, 2006; Grimes, 2007; Paulose *et al.*, 2007). The high efficiency of TiO<sub>2</sub> as a photoelectrode in a PEC water splitting cell requires a suitable architecture that minimizes electron loss at nanostructure connections and maximizes photon absorption (Mahajan *et al.*, 2008; Dholam *et al.*, 2009; Sun *et al.*, 2010). In order to further improve the immigration of photo-induced charge carriers, considerable effort has to be exerted to further improve the water splitting performance under visible light illumination (Knorr *et al.*, 2008; Li *et al.*, 2010). Lately, interesting and unique features of WO<sub>3</sub>-TiO<sub>2</sub> binary oxide photocatalyst system have gained much attention and became favourite research matter among various groups of scientists. The relationship between the WO<sub>3</sub> on

TiO<sub>2</sub> photocatalyst as well as their PEC water splitting performance was still a matter of debate and remains unclear. It was noted that the properties of this binary oxide primarily depend on the nature of the preparation method and the role of optimum WO<sub>3</sub> content incorporated into the TiO<sub>2</sub>. Therefore the development of efficient visible light responsive photocatalyst remains to be determined. In the subsequent section, the historical overview, basic principal, material selection and work done by various researchers with regards to the TiO<sub>2</sub> nanotubes as well as WO<sub>3</sub>-TiO<sub>2</sub> nanotubes applied in PEC water splitting application will be reviewed in detail.

## **2.2 Historical overview of PEC water splitting**

As the drive to seek alternative energy sources significantly increases across the world, there is a growing interest in low-cost, easily manufactured, and high efficiency energy sources (Kreuter and Hofmann, 1998). One of those sources is the harnessing of the sun light energy through the excitation of semiconductor materials, later coined as semiconductor photocatalyst (Aroutiounian *et al.*, 2005; Barreca *et al.*, 2011; Tong *et al.*, 2012). The early work on semiconductor photocatalysis was reported by Becquerel (1839). He reported that a silver chloride electrode connected to a counter electrode and immersed in an electrolyte solution, generates a voltage and an electric current during illumination of sunlight. The discovery that the energy of sunlight can be captured and converting into electric power had brought out lots of great ideas for scientists and researchers, whom seek alternative energy sources. Later, the photoelectric effect was first applied to a device by Charles Fritts (1883) with the development of a selenium and gold *pn* junction device with approximately 1% efficiency. However, the literature regarding to the photocatalyst was limited at the early part of the last century.

In 1954, the first *pn* junction solar cell design was published and reported by Bell Laboratories with an efficiency of 6% (Chapin *et al.*, 1954). The innovation by Bell Laboratories produced the first viable commercial solar cell, which has been revolutionized the photovoltaic industry. Since then, the improvements have been made to give photovoltaic more accessibility in the global energy market. The conversion of sunlight to electrical power has been dominated by solid-state junction devices, often made of silicon (Solanki, 2009; Okamoto *et al.*, 2011). However, this dominance is now being challenged by the emergence of the new generation of PEC water splitting cell (integration of photovoltaic system with an electrolyzer to generate clean and portable H<sub>2</sub> energy carrier). The main disadvantage of the photovoltaic is that it does not operate well at night or during the period of bad weather. Thus, storage of energy as chemical fuel in the H<sub>2</sub> form is essential (Grätzel, 2001; Currao, 2007; Barreca *et al.*, 2011).

The energy can be stored in H<sub>2</sub> fuel within a fuel cell can then be efficiently converted into electrical energy and to be available at all times. This cell normally is based on nanocrystalline materials, which offers the prospect of cheap fabrication together with other attractive feature such as high chemical stability and flexibility in aqueous solution under evolving O<sub>2</sub>. Those materials also have reasonably high incident light to current generation when operated in a PEC water splitting cell (Grätzel, 2001; Grimes *et al.*, 2007; Allam *et al.*, 2008; Centi and Perathoner, 2009). In 1972, Fujishima and Honda discovered the PEC water splitting process for H<sub>2</sub> generation using TiO<sub>2</sub> electrodes. This breakthrough has triggered the subsequent interests in photocatalysis research by scientists and researchers from all over the world on TiO<sub>2</sub> and made TiO<sub>2</sub> as an important component in many practical applications.

### 2.3 Basic principle of PEC water splitting

PEC water splitting process is the general term for a chemical reaction in which water is separated into O<sub>2</sub> and H<sub>2</sub> using photocatalyst that catalyze the water splitting reaction. A basic schematic diagram of such overall water splitting reaction using a semiconductor photocatalyst is presented in Figure 2.1.

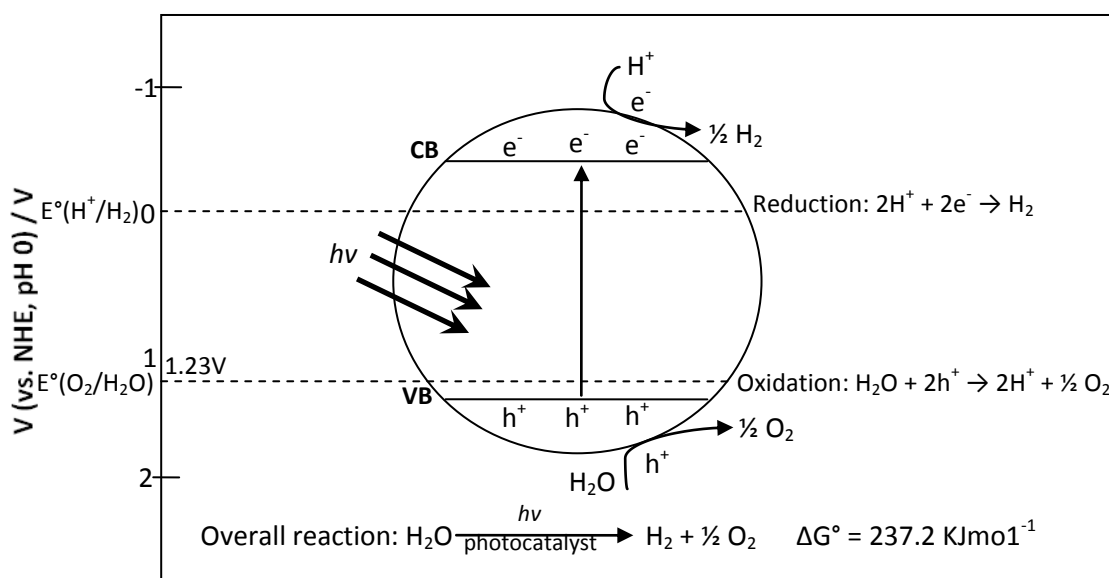
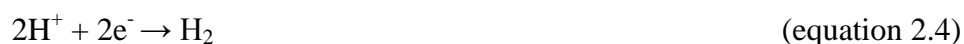


**Figure 2.1:** Basic principle of the overall water splitting reaction on a semiconductor photocatalyst (Leung *et al.*, 2010).

The overall water splitting reaction is considered as a thermodynamically uphill reaction with a large a Gibbs free energy of  $\Delta G^0 = + 237.2 \text{ KJ mol}^{-1}$  (equation 2.1). This indicates that photon energy is required to overcome the large positive change in Gibbs free energy through PEC water splitting (Leung *et al.*, 2010). The light-driven water splitting process is triggered when n-type TiO<sub>2</sub> photocatalyst absorbs photons ( $h\nu$ ) with energies greater than its band gap energy. This light absorption generates electrons in the conduction band and holes in the valence band (equation 2.2). The holes perform work at the TiO<sub>2</sub> electrolyte interface oxidizing water molecules to create O<sub>2</sub> and H<sup>+</sup> ions (equation 2.3). The electrons will move

through the external circuit to the platinum electrode where they reduce  $H^+$  ions creating  $H_2$  molecules due to the electric field or under external bias (equation 2.4).



If these reactions are to proceed with success, the band gap of the semiconductor photocatalyst must satisfy certain requirements. It is necessary that the photon delivering energy to the reaction has enough energy to perform both the oxidation and reduction reactions of water on its surface. In the case of PEC water splitting, this means that the incoming energy must be at least equilibrium with cell potential for water electrolysis, which is 1.23 eV at 25 °C and 1 atm.

A Schottky contact is formed between metal (Ti foil) and semiconductor ( $TiO_2$  nanotubes) as presented in Figure 2.2. In this manner, Fermi level must be constant throughout the sample; otherwise no electric current will flow. A potential gradient along the interface is formed and then will lead to the band bending. Thus, photo-induced electrons will force to transfer from semiconductor to the metal. Then, these photo-induced electrons will drift to the counter electrode and reduce the  $H^+$  ions into  $H_2$  gases under external bias.

However, there is unavoidable energy losses associated with any solar energy conversion process involving semiconductor photocatalyst. When solar illumination strikes the photocatalyst, any photons absorption with the energy higher than band gap of the photocatalyst will excite the electrons from the valence band into conduction band. In this case, recombination of electron/hole pairs can be acted very rapid and release energy in the form of unproductive heat or photons (Grimes *et al.*, 2007). Other possible reasons for the energy losses includes electrons transport

within the sample during charge carriers separation, transport of electrons from photoanode to counter electrode, and Joule heating due to the electrons flow through the external circuit (Leung *et al.*, 2010). In a practical PEC water splitting system, energy losses can be greater than 0.8 eV (Ni *et al.*, 2007; Navarro Yerga *et al.*, 2009). Thus, the optimum band gap of semiconductor photocatalyst applied to PEC water splitting cell must be approximately 2.0 eV (Grimes *et al.*, 2007).

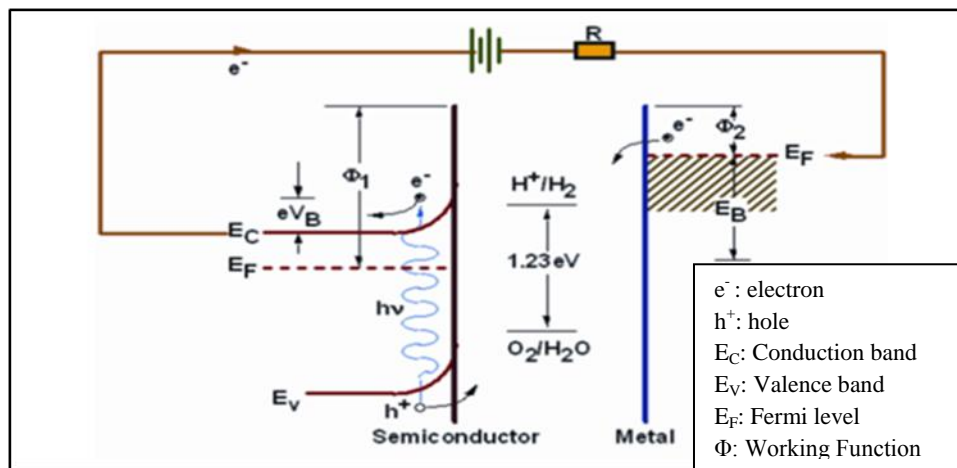


**Figure 2.2:** Energy diagram for an n-type semiconductor-metal in photoelectrolysis cell (Neelkanth *et al.*, 2009).

However, there is unavoidable energy losses associated with any solar energy conversion process involving semiconductor photocatalyst. When solar illumination strikes the photocatalyst, any photons absorption with the energy higher than band gap of the photocatalyst is lost as heat. There is only a partial fraction of the excited state energy can be used to separate electrons from their atomic bonds to produce electron/hole pairs (Grimes *et al.*, 2007). Other possible reasons for the energy losses includes electrons transport within the photoanode during charge carriers separation, transport of electrons from photoanode to platinum electrode, and Joule heating due to the electrons flow through the external circuit (Leung *et al.*, 2010). In a practical PEC water splitting system, energy losses can be greater than 0.8 eV (Ni *et al.*, 2007; Navarro Yerga *et al.*, 2009). Thus, the optimum band gap of semiconductor

photocatalyst applied to PEC water splitting cell is approximately 2.0 eV (Grimes *et al.*, 2007).

#### 2.4 Material selection for PEC water splitting

Taking into account of the processes involved in the dissociation of water on particulate photocatalysts under visible light irradiation, the materials used as photocatalysts must satisfy several functional requirements with respect to band gap energy and electrochemical properties as shown below:

- i. Band edge position: The conduction band level should be more negative than H<sub>2</sub> production level ( $E_{\text{H}_2/\text{H}_2\text{O}}$ ) while valence band level should be more positive than water oxidation level ( $E_{\text{O}_2/\text{H}_2\text{O}}$ ) for efficient H<sub>2</sub> generation (Ni *et al.*, 2007).
- ii. Band-gap: The electronic band gap should be low for most of the solar light spectrum so that can be used for photoexcitation (Misra *et al.*, 2009).
- iii. Transportation of charge carriers: Charge carriers should be transported with minimal losses from the bulk oxide material to the counter electrode for high efficient H<sub>2</sub> generation. (Grimes *et al.*, 2007).
- iv. Stability: The photocatalyst must be stable against photocorrosion in electrolyte (Misra *et al.*, 2009).

Besides, light-harvesting ability of a photocatalyst is an important criterion to produce maximum photo-induced charge carriers. The basic parameter that governs the light-harvesting ability of the photocatalyst is its electronic structure, which determines its band gap energy. Various wide band-gap metal oxide semiconductor (TiO<sub>2</sub>, WO<sub>3</sub>, ZnO, Fe<sub>2</sub>O<sub>3</sub>, SnO<sub>2</sub>, SiC) and non-oxide semiconductors (CdS, CdSe,

GaAs, GaP) have been identified as attractive materials for stable and highly efficient renewable energy devices (Ahn *et al.*, 2007; Marsen *et al.*, 2007). Figure 2.3 illustrates the positions of band edges of various semiconductors regarding to the normal hydrogen electrode (NHE) as standard for zero potential for water-oxidation/reduction processes. As viewed from the band positions, CdSe, CdS, ZnO, TiO<sub>2</sub> and SiC fulfill the thermodynamic requirements for overall water splitting.

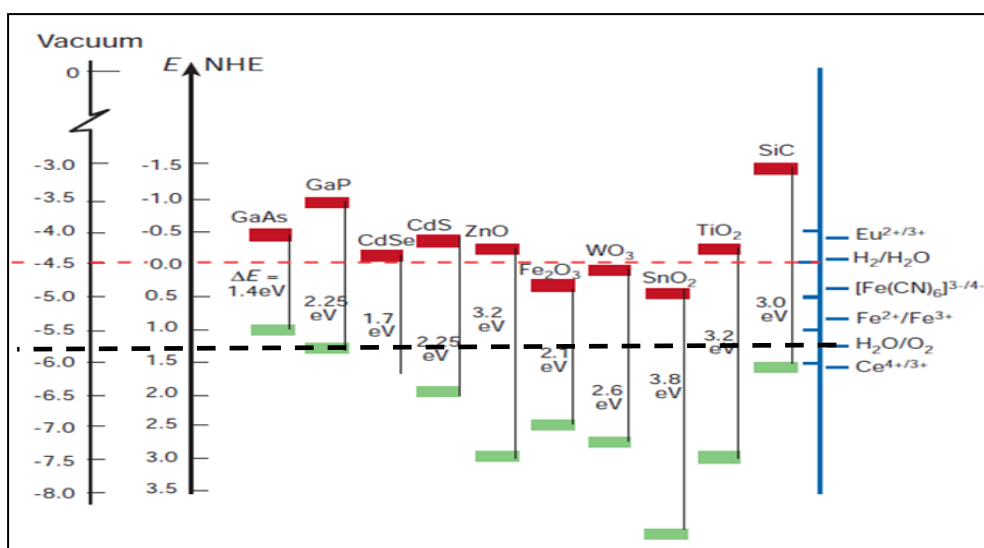


**Figure 2.3:** Electronic structure of different semiconductors and the relative position of their band edge vs. some key redox potentials (Grätzel, 2001).

Among these semiconductors, CdS and CdSe showed lower band gap and suitable band edge position. However, CdS, and CdSe are unstable in the water oxidation reaction because anions of these materials are more susceptible to oxidation than water, causing both (i.e., CdS and CdSe) to degrade by oxidation (Neelkanth *et al.*, 2009, Ni *et al.* 2007). ZnO fulfills the thermodynamic requirements for PEC water splitting reactions. However, ZnO is more likely to form nanowires and nanorods with random distribution arrangement as well as difficult to grow into self-organized and highly order nanotubes architecture. In this manner, ZnO nano-architecture will result in inadequate light absorption, higher surface recombination and limit its practical application in PEC water splitting. Among all of the available



semiconductor photocatalysts, TiO<sub>2</sub> offers great promise for PEC water splitting applications and it is perfectly suitable as a photoelectrode in PEC water splitting system, which has a positive impact on the PEC utility of the material (Misra *et al.*, 2009; Leung *et al.*, 2010; Nah *et al.*, 2010).

## **2.5 TiO<sub>2</sub> photocatalyst for PEC water splitting**

In 1972, PEC water splitting using TiO<sub>2</sub> as photoelectrode was successfully reported by Fujishima and Honda. Since then, TiO<sub>2</sub> has been extensively used as an efficient photoelectrode in PEC water splitting system for H<sub>2</sub> generation because of its unique characteristics (Kitano *et al.*, 2007; Shankar *et al.*, 2008; Dholam *et al.*, 2008; Yan and Zhou, 2011). Particles/spheres of TiO<sub>2</sub> as photoelectrode in PEC water splitting system has been reported in earlier studies, either freely suspended in solution or compacted to a robust photoelectrode. However, the drawbacks of such photoelectrode include the presence of defects or trapping sites, more grain boundaries, and disordered contact areas between two particles/spheres (Sun *et al.*, 2010; Roy *et al.*, 2011). Hence, the electron transporting time in the bulk phase of TiO<sub>2</sub> particles/spheres is rather long, which leads to more recombination losses and scattering problems of photo-induced electrons. Furthermore, the use of TiO<sub>2</sub> particle/sphere photoelectrode requires appropriate substrates as support for the catalysts in PEC system to ease the filtration procedure after photoreaction (Yang *et al.*, 2010). Recently, two-dimensional TiO<sub>2</sub> thin film photoelectrode has been used in PEC water splitting system because of their capability to eliminate the above listed problems and still be reusable (Ghicov and Schmuki, 2009; Liu *et al.*, 2011; Sun *et al.*, 2011). However, two-dimensional TiO<sub>2</sub> thin film photoelectrode generally does not possess large active surface area for PEC reactions (Yang *et al.*, 2010). Therefore, maximizing the specific surface area of TiO<sub>2</sub> thin film is crucial. 1D TiO<sub>2</sub> nanotube

arrays are considered an ideal photoelectrode because of their inner and outer wall surface area of nanotube that greatly increases the density of the active sites available for photon absorption (Nah *et al.*, 2010; Zhang *et al.*, 2010; Krengvirat *et al.*, 2012; So *et al.*, 2012). Therefore, the use of 1D TiO<sub>2</sub> nanotubes is much better and effective way to improve the PEC water splitting performance.

Synthesis of 1D TiO<sub>2</sub> nanostructures can be achieved by various approaches such as sol-gel synthesis (Hoyer *et al.*, 1996; Liu *et al.*, 2000; Yuan and Su, 2004), hydrothermal synthesis (Kasuga *et al.*, 1999; Zhang *et al.*, 2004; Kasuga, 2005), and anodization technique (Mor *et al.*, 2003; Mishra *et al.*, 2003; Mor *et al.*, 2006; Paulose *et al.* 2006). Among all of these methods, anodization technique is the most feasible due to its ability to create self-organized anodic oxides in the form of nanotubular structures with almost perfect vertical alignment. Moreover, anodization is relatively simple and can be adopted for large-scale industrial production (Macak *et al.*, 2006; Ghicov and Schmuki, 2009). Most importantly, 1D TiO<sub>2</sub> nanotube arrays provides a unidirectional electrical channel for photo-induced charge carrier transfer, at where TiO<sub>2</sub> grains are stretched in the tube growth direction. Thus, vertical transportation of charge carriers could be enhanced and improved the PEC water splitting performance due to low recombination losses at grain boundaries (Roy *et al.*, 2011). In order to get the right dimensions and morphologies, a controlled synthesis procedure for the production of nanotube arrays must be investigated and optimized by tuning the length, wall thickness, pore diameter, and intertube spacing through the synthesizing process. However, massive organic waste will be produced after the anodization process, thus, proper organic waste management and disposal is required. In the following section, TiO<sub>2</sub> nanotube arrays and the formation by various authors will be reviewed.

## 2.6 TiO<sub>2</sub> nanotube arrays

Highly ordered and self-aligned 1D TiO<sub>2</sub> nanotube arrays is commonly produced by anodization method (Paulose *et al.*, 2007; Macak *et al.*, 2008). Vertically oriented nanotube arrays offer large specific surface area, which have tube-like structures with circular nanotubular opening serve as a scaffold to anchor light-harvesting assemblies (Grimes, 2007; Sun *et al.*, 2010). The diameter of the opening ranges from 20 nm to 350 nm and the length of the tube can vary from 0.2  $\mu\text{m}$  to 1000  $\mu\text{m}$  depending on the processing parameter. The bottom part of the nanotubes which are in the form of domes is called barrier layer with typical shape of hexagonal or pentagonal (Mohapatra *et al.*, 2007). Figure 2.4 shows FESEM images of the cross section, top viewed and bottom part of typical self organized TiO<sub>2</sub> nanotube arrays, respectively. The formation of nanotubes by anodization technique will be reviewed in the preceding section.

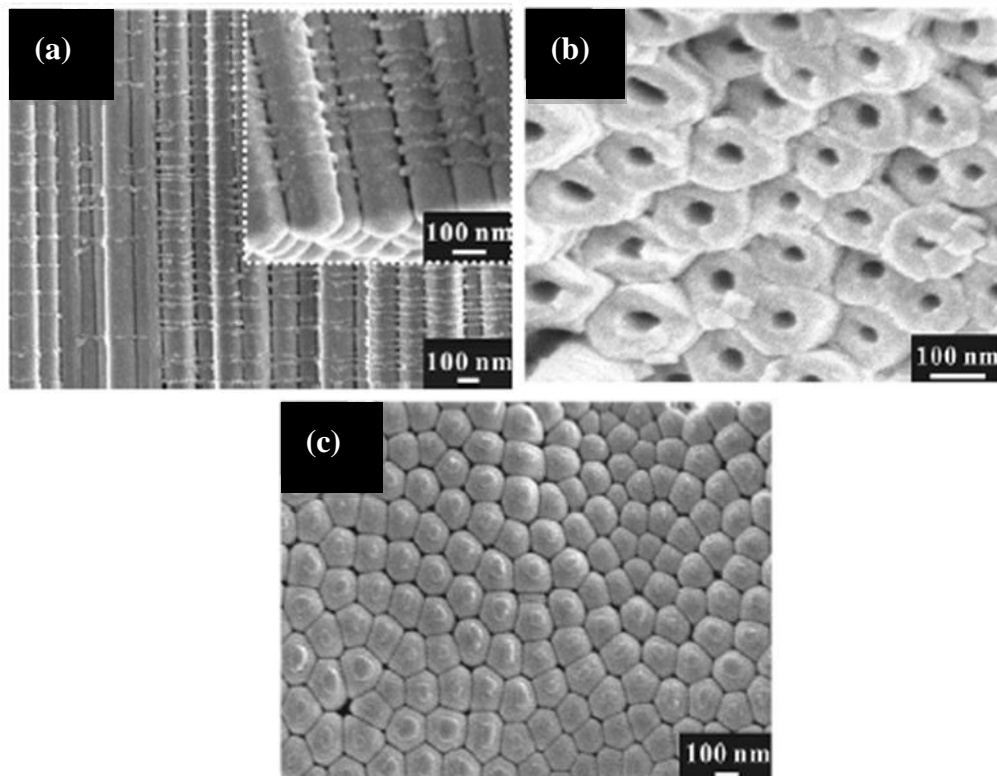


**Figure 2.4:** SEM images of (a) cross sectional image of TiO<sub>2</sub> nanotubes, inset is the image with higher magnification, (b) top view of TiO<sub>2</sub> nanotubes, and (c) bottom of TiO<sub>2</sub> nanotubes (Zhang *et al.*, 2010).

### 2.6.1 Formation of TiO<sub>2</sub> nanotube arrays

Ti foil can be used to grow an oxide film via electrochemical process. In anodizing cell, Ti is used as an anode and it is connected to positive terminal of power source, whereas platinum is used as cathode and being connected to negative terminal of power source. There are few other candidates for cathode, which consist of carbon, lead, nickel or stainless steel. The cathode has to be an inert electrode and non-reactive in the electrolyte bath (Mor *et al.*, 2006; Allam and Grimes, 2008). Figure 2.5 shows a typical experimental setup of anodization and typical structure of TiO<sub>2</sub> nanotubes after anodization process. When the circuit is connected, electrons will flow from the anode, allowing the ions on the metal surface to react with electrolyte to produce oxide layer on the metal. During anodization process, magnetic stirring is commonly used to reduce the thickness of the double layer at the Ti foil/electrolyte interface, and ensure the uniform local current density as well as temperature over the Ti electrode (Macak *et al.*, 2006, Paulose *et al.*, 2006). The electrochemical condition such as voltage, time, concentration of electrolyte, temperature, and pH of electrolyte will determine the morphological and structural of TiO<sub>2</sub> nanotubes (Muti *et al.*, 2008). In the next section, synthesis generations of TiO<sub>2</sub> nanotubes formation are discussed and several mechanism models are presented.

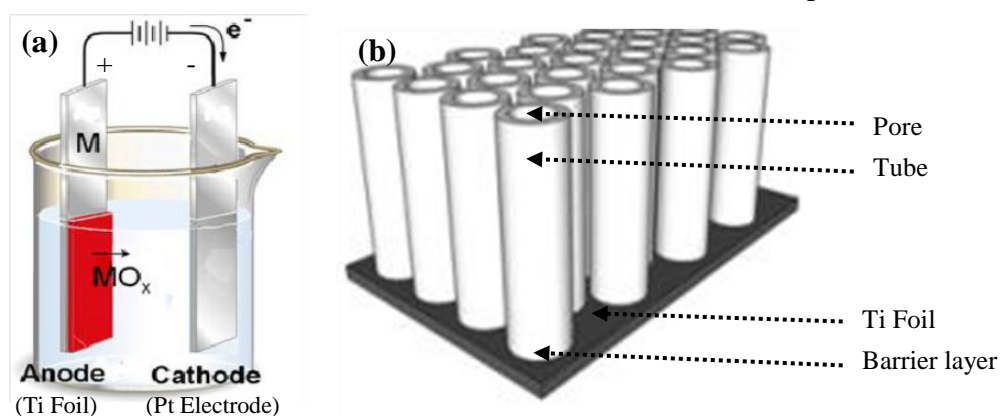


**Figure 2.5:** (a) Typical experimental setup of anodization system and (b) schematic diagram of the typical structure of TiO<sub>2</sub> nanotubes after anodization process (Macak *et al.*, 2007).

### 2.6.2 The four synthesis generation of TiO<sub>2</sub> nanotubes

The first generation of the TiO<sub>2</sub> nanotube arrays synthesis was achieved by aqueous electrolytes (HF-based electrolyte), such as HNO<sub>3</sub>/HF, H<sub>2</sub>SO<sub>4</sub>/HF, H<sub>2</sub>CrO<sub>7</sub>/HF, H<sub>2</sub>SO<sub>4</sub>/NH<sub>4</sub>F and CH<sub>3</sub>COOH/NH<sub>4</sub>F electrolyte. A report in 1999 by Zwilling and co-workers suggested that self-organized porous TiO<sub>2</sub> can be obtained by anodizing a Ti-based alloy in an acidic, fluoride-based electrolyte. In 2001, Gong and co-workers fabricated a form of self-organized, highly uniform TiO<sub>2</sub> nanotubes by anodizing Ti in an aqueous electrolyte that contains dilute HF. Maximum nanotube lengths in this first synthesis generation were approximately 500 nm. It was found that the short nanotubes mainly attributed to the higher surface etching rate at the tip of nanotubes due to the excessive H<sup>+</sup> ions in the electrolyte.

In the second generation, the length of TiO<sub>2</sub> nanotubes was increased to approximately 7 μm by controlling the pH of the electrolyte. Cai and co-workers (2005) were first to fabricate TiO<sub>2</sub> nanotubes of several μm in length using KF and NaF electrolytes by varying electrolyte pH. They found that the difference in electrolyte pH, in turn controlled the surface etching rate at the tip of the nanotubes and chemical dissolution rate at the barrier layer of nanotubes. This condition leads to significant variation in tube length and pore diameter.

In the third-generation, TiO<sub>2</sub> nanotubes with lengths of up to approximately 1000 μm were achieved using non-aqueous and polar organic electrolytes such as formamide, dimethylsulfoxide, ethylene glycol or diethylene glycol (Ruan *et al.*, 2006). The key for successfully growing long nanotube arrays was to keep the water content below 5 wt% in the anodization bath. A few studies discovered that the addition of optimum amount of water results in high growth rate (i.e., over 10 nm/min) of organic electrolyte (Poulose *et al.*, 2006; Prakasam *et al.*, 2007; Raja *et*

*al.*, 2007; Sohn *et al.*, 2008; Chang *et al.*, 2009; Wan *et al.*, 2009). In those studies, water was observed to act as an oxygen provider, which supplied sufficient amount of  $O^{2-}$  ions needed for oxidation. Besides, the use of high fluoride content in an organic electrolyte containing optimum amount of water was noticed to accelerate the chemical dissolution at the bottom of the nanotubes, resulting in longer nanotube arrays (Paulose *et al.*, 2006; Shankar *et al.*, 2007; Sreekantan *et al.*, 2010).

The fourth synthesis generation was non-fluoride-based anodization chemistries. In 2006, Nakayama *et al.* reported the formation of  $TiO_2$  nanotubes by anodization in a perchloric acid solution. Richter *et al.* (2007) grew similar nanotubes in oxalic acid, formic acid, and sulfuric acid solutions containing 0.3–0.6 M  $NH_4Cl$ . However, the nanotubes were in bundles form rather than arrays. The length of nanotubes was approximately 60  $\mu m$ . There was no obvious dependence of nanotube diameter upon voltage; all tubes diameters were between 15 and 35 nm with wall thickness of about 5 nm (Hahn *et al.*, 2007). The finding indirectly showed the importance role of the fluoride ions in the formation of well-aligned and highly ordered nanotube arrays. Therefore, in the present work, organic electrolyte containing fluoride ions was used for producing  $TiO_2$  nanotube arrays.

### **2.6.3 Mechanism of formation of $TiO_2$ nanotubes**

In this section, the formation mechanisms of  $TiO_2$  nanotubes proposed by various authors are reviewed. There are mainly three mechanistic models of  $TiO_2$  nanotubes formation via anodization technique. In early 2004, Choi *et al.* developed a mechanistic model of  $TiO_2$  nanotube formation by describing the formation of porous  $TiO_2$  due to electrical breakdown of the  $TiO_2$  (Figure 2.6). Initially, the barrier layer of  $TiO_2$  was developed and grows thicker with increasing applied anodization